



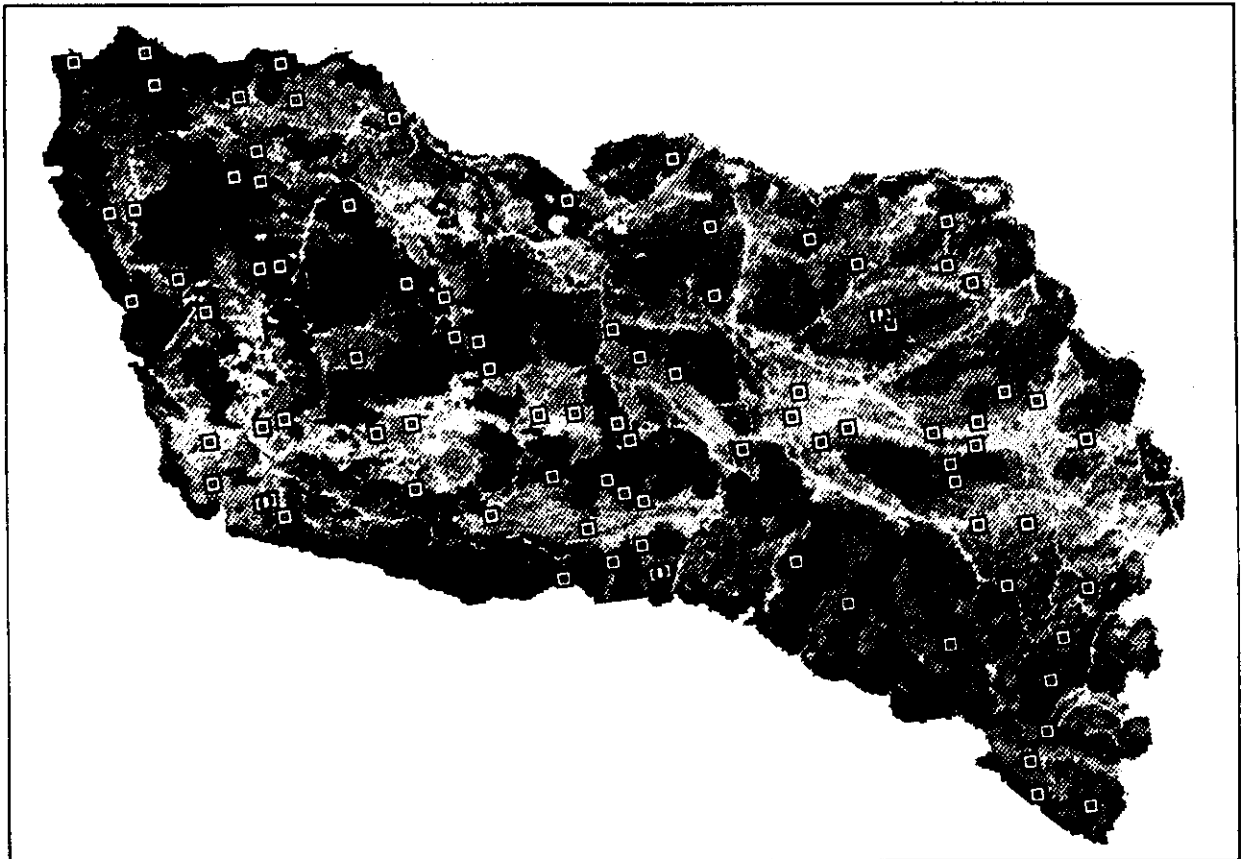
US Army Corps  
of Engineers

Construction Engineering  
Research Laboratories

USACERL Special Report (SR) EC-94/28  
August 1994

# Using Neural Networks To Correlate Satellite Imagery and Ground-truth Data

by  
Xiping Wu  
James D. Westervelt



Current approaches to evaluating the condition of natural resources on Army training and testing lands are statistically based and attempt to generate rational mathematical formulae that characterize the relationship between satellite imagery and ground-truth data. Even in the hands of a well trained image processing expert, the application of standard image processing tools can yield varying results.

Army land managers need an alternate approach for correlating satellite imagery to ground-truth measurements. This approach can be found in the application of neural networks.

This report presents the research results of using neural networks as a computational tool to correlate ground-truth data with satellite imagery for Hohenfels, Germany, and to turn the imagery into maps of the installation.

Approved for public release; distribution is unlimited.



## Foreword

This report was funded by the U.S. Army Construction Engineering Research Laboratories (USACERL) under the In-Laboratory Independent Research (ILIR) Program.

Xiping Wu is a postdoctoral research associate from the Department of Civil Engineering at the University of Illinois. Appreciation is expressed to Professor J. Ghaboussi of the Department of Civil Engineering at the University of Illinois; Susan Ribanski, Oak Ridge Affiliate Universities working at USACERL; and Michael Shapiro, and David J. Tazik of USACERL, for discussions and help provided during this study. The authors would also like to thank the following Land Condition Trend Analysis (LCTA) personnel: Steve Warren, Pam Sydelko, Julie Wentz, Cal Bagley, Bob Brozka, Paul Dubois, Lyle Trumball, and Jeff Courson. Special appreciation is expressed to John Brent and Bernt Weber of the Natural Resources staff at Hohenfels, Germany.

The work was monitored by the Environmental Compliance Modeling and Systems Division (EC) of the Environmental Sustainment Laboratory (EL), U.S. Army Construction Engineering Research Laboratories (USACERL). James D. Westervelt, was the principal investigator. Dr. John T. Bandy is Chief, CECER-EC, and Dr. William D. Goran is Chief, CECER-EL. The USACERL technical editor was Gloria J. Wienke, Information Management Office.

LTC David J. Rehbein is Commander and Acting Director of USACERL, and Dr. Michael J. O'Connor is Technical Director.

# Contents

<b>SF 298</b> .....	1
<b>Foreword</b> .....	2
<b>List of Figures and Tables</b> .....	4
<b>1 INTRODUCTION</b> .....	7
Background .....	7
Objectives .....	8
Approach .....	8
<b>2 NEURAL NETWORKS</b> .....	10
Introduction .....	10
Backpropagation Neural Networks .....	11
Adaptive Simulation of Multilayer Feedforward Neural Networks .....	13
<b>3 DEVELOPMENT OF CORRELATORS</b> .....	17
A Neural Network-Based Approach .....	17
Development of Neural Network-Based Correlators .....	19
Comparison With the Theoretical Approach .....	21
<b>4 CONCLUSIONS AND RECOMMENDATIONS</b> .....	49
<b>REFERENCES</b> .....	51
<b>DISTRIBUTION</b>	

## List of Figures and Tables

### Figures

1	A Sample Backpropagation Neural Network .....	15
2	The Dynamic Node Creation Process .....	16
3	Architecture of the Neural Network for Percent Land Coverage Prediction .....	24
4	Prediction of Percent of Land Cover (%LC) From the Neural Network With 40 Training Data Sets .....	25
5	Prediction of Percent of Land Cover (%LC) From the Neural Network With 60 Training Data Sets .....	26
6	Prediction of Percent of Land Cover (%LC) From the Neural Network With 80 Training Data Sets .....	27
7	The Map of Percent of Land Cover (%LC) Predicted by the Neural Network .....	28
8	Prediction of Percent of Bare Ground (%BG) From the Neural Network With 40 Training Data Sets .....	29
9	Prediction of Percent of Bare Ground (%BG) From the Neural Network With 60 Training Data Sets .....	30
10	Prediction of Percent of Bare Ground (%BG) From the Neural Network With 80 Training Data Sets .....	31
11	The Map of Percent of Bare Ground (%BG) Predicted by the Neural Network ...	32
12	Prediction of Percent Disturbance (%DIST) From the Neural Network With 40 Training Data Sets .....	33
13	Prediction of Percent Disturbance (%DIST) From the Neural Network With 60 Training Data Sets .....	34
14	Prediction of Percent Disturbance (%DIST) From the Neural Network With 80 Training Data Sets .....	35

15	The Map of Percent Disturbance (%DIST) Predicted From the Neural Network With 60 Training Data Sets . . . . .	36
16	The Map of Forest Presence Predicted by the Neural Network . . . . .	37
17	Prediction of Percent Clay (%CLAY) From the Neural Network With 40 Training Data Sets . . . . .	38
18	Prediction of Percent Clay (%CLAY) From the Neural Network With 60 Training Data Sets . . . . .	39
19	Prediction of Percent Clay (%CLAY) From the Neural Network With 80 Training Data Sets . . . . .	40
20	Prediction of Percent Sand (%SAND) From the Neural network With 40 Training Data Sets . . . . .	41
21	Prediction of Percent Sand (%SAND) From the Neural Network With 60 Training Data Sets . . . . .	42
22	Prediction of Percent Sand (%SAND) From the Neural Network With 80 Training Data Sets . . . . .	43
23	Prediction of Percent Silt (%SILT) From the Neural Network With 40 Training Data Sets . . . . .	44
24	Prediction of Percent Silt (%SILT) From the Neural Network With 60 Training Data Sets . . . . .	45
25	Prediction of Percent Silt (%SILT) From the Neural Network With 80 Training Data Sets . . . . .	46
26	The Map of Percent Clay Predicted by the Neural Network . . . . .	47
27	Comparison of Theoretical and Neural Network Results for Percent Land Cover . . . . .	48

#### Tables

1	The Training and Testing Results for Forest Classification . . . . .	21
2	Linear Regression Values for Comparing Model Predictability . . . . .	24

# 1 INTRODUCTION

## Background

To monitor the condition of natural resources on Army training and testing lands, the U.S. Army Construction Engineering Research Laboratories (USACERL) developed the Land Condition Trend Analysis (LCTA) program. LCTA is a component of the overall Integrated Training Area Management (ITAM) program. As part of the LCTA process, sample plots are scattered in a stratified random fashion across training lands at an Army installation based on soil types and land cover categories generated by an unsupervised classification of satellite imagery. Sample plots are 100 by 6 meters (m) in size. Plant cover is determined by point intercept along a 100-m transect that forms the longitudinal axis of the plot. Woody plant density is determined by counting all individual plants in the plot or subplot. Soil samples are collected, topographic features are recorded, a floristic survey is conducted and the presence of wildlife is recorded. These methods are documented in Tazik et al. (1992). Information regarding total plant cover, percent bare ground, and percent disturbance is calculated for each plot. These values are then correlated with satellite imagery in an attempt to extrapolate plot data across the entire installation.

Current approaches to evaluating the condition of natural resources are statistically based and attempt to generate rational mathematical formulae that characterize the relationship between satellite imagery and transect values. These approaches use the image data in conjunction with knowledge of the image access time, satellite orientation, sun orientation, atmospheric conditions, time of year, and weather conditions. Even in the hands of a well trained image processing expert, the appropriate application of standard image processing tools can take many forms, and yield different results.

An alternate approach for correlating imagery to ground-truth measurements can be found in the field of neural networks. Research in neural networks, a paradigm for computation and knowledge representation inspired by the neuronal architecture and operation of the human brain, has experienced a considerable resurgence of interest in recent years, although its foundation was laid in the 1940's. This renewed interest is supported by the realization that neural computing is inherently parallel, and it has the capability of learning or self-

organization. Moreover, new insight in the learning algorithms in recent years has advanced the technology and raised the modeling power of neural networks to a new level. With the advance and sophistication in some branches of neural networks, this technology has been successfully applied to a number of fields, especially in pattern recognition, image processing, functional modeling, and even image classification with remotely sensed data.

The resurgence in research in neural networks has facilitated the development of a decidedly different approach to correlating satellite imagery and ground-truth data. With a neural network approach, the correlation can be captured within a multilayer feedforward network through training the network with sampled transect data. The neural network captures the relationship embedded in the data in its weight structures, and no formal mathematical rules or formulae are explicitly observable. As a computational entity, there is no technical barrier to using this model within a graphic information system (GIS) such as the Geographic Resources Analysis Support System (GRASS). This report presents the research results in using neural networks as a computational tool to correlate LCTA transect data with satellite imagery for Hohenfels, Germany, and then, using the relationship in the form of a trained network within GRASS, to turn the imagery into maps covering the entire installation.

## **Objectives**

The main objectives of this research were to investigate the applicability of neural network computing in constructing correlators for SPOT (Systeme Probatoire pour l'Observation de la Terre) satellite imagery and LCTA data, to verify the approach by comparing how well the network predicts land coverage to a theoretical approach, and to study the implementation of neural network-based correlators within GRASS.

## **Approach**

Chapter 2 describes briefly the characteristics and operation of neural networks. The learning procedures and algorithms of backpropagation neural networks, and the adaptive simulation environment used in this study are presented in detail. Chapter 3 addresses the neural network-based modeling methodology to correlate satellite imagery and ground-truth data, the development of neural network-based correlators for LCTA data, and a comparative study with a theoretical approach to the correlation and prediction of percent land coverage condition. Chapter 4

---

summarizes the results of this research and proposes further work in the development of the neural network image process module within GRASS.

## 2 NEURAL NETWORKS

### Introduction

A neural network is a nonlinear dynamic system consisting of a large number of highly inter-connected processing units, or processors. Each processing unit in the network maintains only one piece of dynamic information (its current level of activation) and is capable of only a few simple computations (adding inputs, computing a new activation level, or performing threshold logical calculation). A neural network performs "computation" by propagating changes in activation between the processors; it stores the knowledge it has "learned" as strengths of the connections between its processors. The large number of these processing units, and the high inter-connectivity among them, similar to highly inter-connected neurons in a brain, give the neural networks their capability of knowledge representation. In addition, it is through self-organization or "learning" that a neural network approaches some representation of a particular knowledge or discovers the hidden relationships in data.

According to Rumelhart, Hinton, and Williams (1986), a neural network is generally made up of the following components: (1) a set of processing units, (2) the state of activation of a processing unit, (3) the function used to compute output of a processing unit, (4) the pattern of connectivity among the processing units, (5) the rule of activation propagation, (6) the activation function, and (7) the rule of learning used. The network topology and the form of the rules and functions are all learning variables in a neural network learning system, leading to a wide variety of network types. Some of the well known types of neural networks are: Competitive Learning (Grossberg 1976; Rumelhart and Zipser 1985), the Boltzmann Machine (Hinton, Sejnowski, and Ackley 1984), the Hopfield Network (Hopfield 1982), the Kohonen Network (Kohonen, Barna, and Chrisley 1988), the Adaptive Resonance Theory (ART) (Carpenter and Grossberg 1987), and the backpropagation neural networks (Rumelhart, Hinton, and Williams 1986). Although many other variations of neural networks exist, the backpropagation network and its variants, as a subset of multilayer feedforward networks, are currently the most widely used networks in applications. The following paragraphs describe the salient features and computational properties of backpropagation networks.

## Backpropagation Neural Networks

The backpropagation network is a multilayer feedforward neural network that uses the generalized delta rule as its learning rule. The processing units in a backpropagation neural network, which are similar to McColluch-Pitts neurons with the exception that the output function or activation function is a sigmoidal instead of a threshold step function, are arranged in layers. Each neural network has an input layer, and output layer, and a number of hidden layers. Propagation of activation takes place in a feedforward manner, from input layer to the output layer. The pattern of connectivity and the number of processing units in each layer may vary, with some constraints. No communication is permitted between the processing units within a layer. The processing units in each layer may send their output to the processing units in higher layers. The general architecture of a backpropagation network is shown in Figure 1.\*

The learning process is determined by (1) the network architecture, in which decisions are made on the number of layers, the size or number of nodes in each layer, and the connection schemes between nodes in different layers, and (2) the learning procedures, which include selecting the type of processing units, type of activation function, and learning algorithms.

In a backpropagation network, two computational procedures are involved in a learning cycle: feedforward computation of activations and backward propagation of error signals for modifying connection weights via the generalized delta rule derived by Rumelhart, Hinton, and Williams (1986). If you denote  $2_{ij}$  as the strength or weight of connection between units  $i$  and  $j$ , a feedforward computation proceeds as follows:

1. The units in the input layer receive their activations in the form of an input pattern and this initiates the feedforward process.
2. The processing units in each layer receive outputs from other units and perform the following computations.
  - a. Compute their net input  $N_j$ ,

$$N_j = \sum_{k=1}^M W_{jk} o_k \quad [\text{Eq 1}]$$

---

\* Figures are located at the end of each chapter.

where:  $o_k$  = output from units impinging on unit  $j$ , and  
 $M$  = number of units impinging on unit  $j$ .

b. Compute their activation values from their net input values,

$$a_j = F_j(N_j) \quad [\text{Eq 2}]$$

where  $F_j$  is usually a sigmoid function.

c. Compute their outputs from their activation values. In the neural network type used in this study, the output is the same as the activation value.

$$o_j = a_j \quad [\text{Eq 3}]$$

3. The output values are sent to other processing units along the outgoing connections.
4. This process continues until the processing units in the output layer compute their activation values. These activation values are the output of the neural computations.

The generalized delta rule is basically a steepest descent scheme with constant step length in a network setting, performing a gradient descent on the error function with respect to the weight space. For multilayer feedforward neural networks, the error function is usually a highly nonlinear function defined as:

$$E(w) \equiv \lim_{N \rightarrow \infty} \frac{1}{N} \sum_{k=1}^N E_k \quad [\text{Eq 4}]$$

where  $E_k = |t(x_k) - o(x_k, w)|^2$ ,  $t(x_k)$  is the expected output;  $o(x_k, w)$  is the network prediction, which is a function of the input vector  $x$  and the network weight vector  $w$ , and  $N$  is the number of total training cases. Therefore, the modification of the strengths or weights on the connections with the generalized delta rule is accomplished with the following formulas:

$$\Delta w_{ij} = \eta \nabla E(w_{ij}) = \eta \delta_j o_i \quad [\text{Eq 5}]$$

In this equation,  $\eta$  is a learning constant called the "learning rate" and  $\delta_j$  is the gradient of the total error with respect to the net input at unit  $j$ . At the output units,  $\delta_j$  is determined from the difference between the expected activation  $t_j$  and the computed activation  $a_j$ :

$$\delta_j = (t_j - a_j) F'(N_j) \quad [\text{Eq 6}]$$

where  $F'$  is the derivative of the activation function. At the hidden units, the expected activations are not known a priori. The following equation calculates  $\delta_j$  for the hidden units:

$$\delta_j = \left( \sum_{k=1}^M \delta_k w_{jk} \right) F'(N_j) \quad [\text{Eq 7}]$$

Due to their popularity in applications, multilayer feedforward neural networks have been extensively studied, and their general mapping capability has been well understood. Hecht-Nielsen (1987) uses Kolmogorov's superposition theorem to show the general functional modeling capability of a multilayer feedforward network; Gallant and White (1988) prove that a three-layer network with one hidden layer is capable of embedding a Fourier analyzer and recently Hornik, Stinchcombe, and White (1989) prove that multilayer feedforward networks are universal approximators. The complexity of learning and the mathematical theory of generalization have also been studied in depth by some other researchers (Judd 1990; Wolpert 1990).

### Adaptive Simulation of Multilayer Feedforward Neural Networks

The generalized delta rule performs a search that results in a very slow convergence rate in training.\* On the other hand, for a backpropagation network, the network architecture of the hidden layers cannot be optimally determined a priori. To solve real world problems efficiently, it is imperative to construct a simulator with a fast learning scheme and some ways to determine the network architecture as the training proceeds. To date, extensive research has produced many new learning algorithms with improved learning rates by using either higher order information or heuristic rules (Falhman 1988; Jacobs 1988; Watrous 1987), and mechanisms for dynamic architecture generation and evaluation (Ash 1989; Tenorio and Lee 1989; Karnin 1990).

To efficiently determine the network architecture and training process, an adaptive simulator called DQP (Wu 1991) that implements the quickprop algorithm (Falhman 1988) and a variant of the Dynamic Node Creation scheme

---

\* The search is a gradient descent search in the weight space through minimization of a mean-squared error function.

(Ash 1989), is used in this study. The implemented learning algorithm and hidden nodes creation scheme are briefly described in the following paragraphs.

With heuristic reasoning, Rumelhart, Hinton, and Williams (1986) introduced a momentum factor to the generalized delta rule so that the formula for weight update becomes:

$$\Delta w(t) = -\eta \frac{\partial E}{\partial w(t)} + \alpha \Delta w(t-1) \quad [\text{Eq 8}]$$

where  $\eta$  is the learning rate and  $\alpha$  is the momentum factor, and both of them are assumed constants. In spite of its simplicity, this modification usually results in some improvement on the robustness of the learning performance over the purely gradient descent-based scheme. To adaptively estimate the momentum factor,  $\alpha$ , a learning algorithm called quickprop was proposed by Falhman (1988), in which the formula for weight update becomes:

$$\Delta w(t) = -\eta \frac{\partial E}{\partial w(t)} + \frac{\frac{\partial E}{\partial w(t)}}{\frac{\partial E}{\partial w(t-1)} - \frac{\partial E}{\partial w(t)}} \Delta w(t-1) \quad [\text{Eq 9}]$$

Numerical experiment indicates that the quickprop algorithm is robust in learning, about an order faster than the generalized delta rule in terms of training epochs, and the scheme seems scaled-up well for large problems.

Based on the theoretical conclusion that a three-layer feedforward network is a universal approximator (Hornik, Stinchcombe, and White 1989), Ash developed the Dynamic Node Creation scheme within backpropagation networks, by fixing the network architecture to three layers with one hidden layer, starting training with one hidden node, and adding one hidden node at a time during a certain training period until the convergence of learning is realized. When a hidden node is added to the hidden layer, connections from this node to all the other input and output nodes are created, and the connection weights initialized. The criterion for adding a new hidden node is governed by the condition that the currently estimated average error slope over a certain number of epochs be less than a predefined gradient tolerance called the "trigger slope." Though this scheme appears to be robust and slightly faster than a standard backpropagation algorithm for training the encode/decode problems, the proper selection of the trigger slope plays an important role in the ultimate performance. However, this

scheme is simple to use and usually results in a quasi-optimal architecture. The dynamic node generation process is schematically illustrated in Figure 2.

With the above observation, a heuristic node-adding rule is developed in this study for the preliminary stage of training, in which the trigger parameter is defined as a percentage of correct predictions over the total training cases. After the network has settled in the solution space (about 80 percent correct prediction), the architecture adjusting is manually controlled. The training process converges when both the maximum absolute error and the total error are below their respective tolerances.

The performance of DQP has been investigated on a large set of benchmark problems and modeling of some chaotic time series predictions (Wu 1991). The compound approach appears to be efficient and robust in modeling real value functions. It not only has a faster learning convergence rate than the generalized delta rule, but also determines the network architecture as the training progresses.

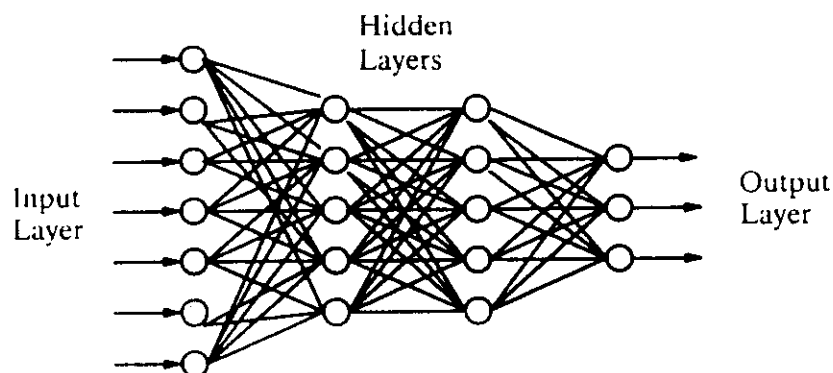
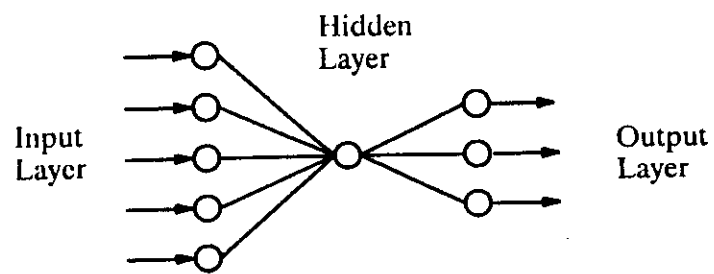
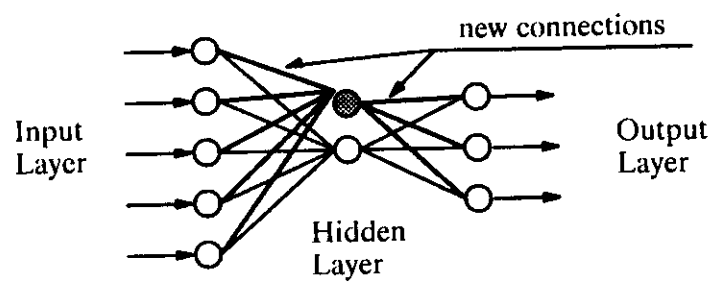


Figure 1. A Sample Backpropagation Neural Network.



(a) The initial Architecture of a Neural Network



(b) The Current Architecture after Adding One Hidden Node

Figure 2. The Dynamic Node Creation Process.

### **3 DEVELOPMENT OF CORRELATORS**

#### **A Neural Network-Based Approach**

The basic strategy for developing a neural network-based correlator that captures the relationship between satellite imagery and ground-truth data is to train an error backpropagation type of neural network on the transect values derived from ground-truth data and the raw SPOT satellite images corresponding to these transects. If a relationship between the satellite imagery and transect values from ground-truth data exists, and a comprehensive set of data that characterize the relationship is available, then the trained neural network should contain sufficient information about the embedded correlation. Such a trained network would not only be able to reproduce the training data set with reasonable accuracy, but through generalization it should be able to approximate the transect values directly from satellite imagery that were not processed through the network. The degree of accuracy in this generalization depends on how comprehensive and representative the training data set is.

The training of a backpropagation neural network with appropriate data containing the information of transect values and corresponding satellite imagery is at the heart of this research. A correlator is established after the training is completed and the trained network is appropriately tested on some new sets of data. The data for this study comes from a ground survey and SPOT satellite image that covers the Hohenfels Combat Maneuver Training Center, Germany. The ground-truth data was collected by a team of researchers during August 1988. The SPOT image is dated August 1988 also. Ground-truth data was painstakingly collected on 90 100 x 6 meter transects randomly situated in the study area.

The ground-truth data was processed by the data collection team to provide a whole spectrum of transect values including the percent of the bare ground shaded by vegetation across the entire transect (LC), the percent disturbances (DIST), the percent bare ground (BG), the presence of forest (FOR), the percent clay (CLAY), the percent sand (SAND), and the percent silt (SILT). For each transect value, the corresponding band intensity values at each transect need to be determined. To accomplish this, the satellite image was geographically referenced to a basemap of the region. Each transect was overlaid on this map to obtain the pixel intensity values contained in the transect. Proportional amounts of each pixel were

combined to generate a single representative band intensity value for each transect. At this stage we have, for each transect, a real value such as the percent land cover value and three intensity values representing the three SPOT bands. Thus, the objective is to train the network with the three-band image data and with the corresponding transect value on a backpropagation neural network to capture the correlation between them.

Decisions regarding the neural network architecture and learning algorithms are normally made before training and testing begin. The composition of the input and output layers is solely determined by the problem and representation scheme used. Hence, three input nodes representing the three SPOT bands and one output node representing the transect value (e.g., percent land cover) are used. With the aid of recent theoretical studies on the mapping capability of neural networks (Hornik, Stinchcombe, and White 1989), it was determined that one hidden layer should be used for this research; the size of the hidden layer was determined with the dynamic node creation scheme during training.

Because of the use of the sigmoidal function in the activation calculation, the raw image data and transect values train most efficiently when normalized into the range of 0.10 through 0.90 before they are presented to the network for training and testing. The normalization scheme can be linear or nonlinear; the simple linear scaling schemes used for this study are:

1. Three channels of image data:  $\text{new\_value} = \text{old\_value}/100.0$ ;
2. Percent land cover:  $\text{new\_value} = 0.10 + 0.80 \times \text{old\_value}$ ;
3. Percent of forest:  $\text{new\_value} = 0.10 + 0.80 \times \text{old\_value}$ ;
4. Percent disturbance:  $\text{new\_value} = 0.10 + 0.80 \times \text{old\_value}$ ;
5. Percent bare ground:  $\text{new\_value} = 0.10 + 0.80 \times \text{old\_value}$ ;
6. Percent sand in soil:  $\text{new\_value} = 0.10 + \text{old\_value}$ ; and
7. Percent silt and clay: no scaling.

After preparing the entire data set with the scaling schemes, a sampling procedure selects the training data set randomly from the 89\* sets of data with three sample sizes: 40, 60, and 80. Four replications were done for each sample size. With this approach, the effect of sampling on the training and testing performance of the neural networks can be qualitatively estimated by performing statistical analysis on the results.

---

\* One of the initial 90 sets of transect data was incomplete, reducing the usable data to 89 transects.

When the training and testing on the 89 sets of transect data were completed, the trained neural network that captured the correlation between the satellite imagery and a transect value was then incorporated into GRASS to generate the land coverage condition maps for the entire training area directly from the satellite imagery.

The following section describes the training, testing, and architecture evolution in the development of each neural network-based correlator in detail.

## **Development of Neural Network-Based Correlators**

Procedures used in the development of neural network-based correlators for percent land cover, percent bare ground, percent disturbance, identification of forest, and percent silt, clay, and sand, are essentially the same. Construction of the correlator for satellite imagery and percent land cover (LC) are described in detail in the following paragraphs as an example.

### ***Percent Land Cover (LC)***

The network architecture for correlating the satellite imagery with land cover condition consists of three layers, as shown in Figure 3. The three input nodes represent the three SPOT bands and the one output node represents the percent land cover value. The size of the hidden layer is determined by the dynamic node creation scheme, and varies with the size of the training data set. The hidden layer was started with 10 nodes; the final hidden size was determined to be 18 after the network trained on the entire transect data set (89 sets of data).

To determine the existence of a relationship between the imagery data and percent land coverage value and the generalization capability of the neural network, the network was trained with data sets consisting of randomly selected samples of 40, 60, and 80 transects out of the total 89 sets of data, and tested with the remaining samples in each size category. Four replications were done for each sample size. The training and testing results for a typical sample in each size category, and the corresponding correlation coefficients, are shown in Figure 4. The training results are plotted as triangles and the testing results as filled circles. Graphs (a) through (c) show the training and testing results for a sample size in each of the three size categories for training data, and graph (d) shows the overall performance of the trained neural network in terms of the correlation ( $R^2$  value) between the predicted value and the expected value. The correlations for all the samples are in the range of 0.894 through 0.931. This indicates that a strong relationship exists between the satellite imagery and percent land cover in the transect data

set, which in turn shows that the embedded relationship has been reasonably captured by the neural network after proper training.

The training and testing results for all the four replications in each size category are shown in Figures 4 through 6. In these figures, the expected percent land cover from the original LCTA data set is plotted against that predicted from the neural network, and the correlation for each sampling case is also included. It is obvious that sampling does make some difference in the learning and testing performance of the neural network. However, the effect of sampling is statistically insignificant because the correlation for each sampling run is essentially in the same range (about 0.90). The minor improvement on the correlation with the increase in the size of the training sample indicates that a strong correlation exists between the LCTA data and the imagery, and the correlation is well captured in the neural network model.

To determine the generalization capability of the neural network after training all the transect data sets, the trained neural network shown in Figure 3 was incorporated into GRASS to generate a percent land cover map for the Army training installation in Bavaria, Germany. The prediction of the neural network correlator on the entire image is shown in Figure 7. The percent land cover predicted is acceptably accurate.

#### ***Percent Bare Ground (BG)***

The network architecture for correlating the percent bare ground with SPOT satellite imagery is similar to the one shown in Figure 3. As with the training of percent land cover data, the number of hidden nodes increases as the sample size changes from 40 to 80 sample data sets, and the final number of hidden nodes reaches 18 when the 80-sample data set is trained. The overall performance of the neural networks is illustrated in Figures 8 through 10, where the correlations ( $R_2$  values) between the expected values and network predictions on training different sized samples of data are plotted. The training and testing results for training the four replications of sample sizes of 40, 60, and 80 are also shown. The map shows the percent of bare ground from the neural network correlator constructed from training all the 89 sets of data on the entire image as shown in Figure 11. The prediction appears reasonable.

#### ***Percent Disturbance (DIST)***

With a three-layer network, the correlator for predicting percent disturbance was built with 22 nodes in the hidden layer after the 80 sample data set was trained. The training and testing results for the four replications of sample sizes of 40, 60,

and 80 are shown in Figures 12 through 14. The map in Figure 15 shows the percent disturbance of the training land from the neural network correlator after training all the data sets.

### ***Forest Classification (FOR)***

The correlation and identification of the presence of forest from the imagery and ground-truth data is basically a classification problem. With a three-layer network, the hidden nodes were determined to be 12 after training 80 sets of sample data. The network learned the correlation almost perfectly and the map generated from this correlator predicts very well the presence of forest in the training land, which is shown in Figure 16. Table 1 lists the training and testing results on training four replications of 40, 60, and 80 samples.

### ***Percent Clay (CLAY), Percent Sand (SAND), and Percent Silt (SILT)***

The construction of correlators between the SPOT satellite imagery and percent clay, sand, and silt in the soil was completed in the same manner as the other correlators. All the three networks with one hidden layer required 18 hidden nodes to learn the correlation to some degree. The training and testing results for percent clay are shown in Figures 17 through 19, for percent sand in Figures 20 through 22, and for silt in Figures 23 through 25. The map that shows the distribution of clay in the training land generated from the network is shown in Figure 26.

## **Comparison With the Theoretical Approach**

The neural network-based approach to correlating satellite imagery and ground-truth data is fundamentally different from the traditional approach. Instead of using human idealization and simplification on the data, the neural network-based

**Table 1**  
**The Training and Testing Results for Forest Classification**

Sample Size	Percent of Correct Predictions (%)							
	Training Results				Testing Results			
40	100	97.5	100	100	95.9	98.0	95.9	95.9
60	100	100	98.3	100	96.5	100	96.6	96.6
80	98.8	95.0	97.5	93.8	88.9	100	100	100

correlator was developed through training on the raw transect data and the corresponding satellite imagery. To illustrate the difference between these two approaches and to further verify the validity of the neural network-based correlator, a comparative study was performed using a more traditional approach based on more standard image processing tools on the same data set that had been used for constructing the neural network-based model.

Traditional image processing steps have strong theoretical basis for image manipulation. Spectral vegetation indices (SVI), bidirectional reflectance distribution function (BRDF), and leaf area indices (LAI) are but several theoretically-based operations to help extract vegetation information from images (Jensen 1986; Lillesand and Kiefer 1987). Similarly, other operations are defined for dealing with atmospheric conditions and corrections required due to land topography. Such operations still leave one with processed images containing a tremendous variety of pixel band intensity values, which often are clustered into several categories. These categories are then labeled to suggest a land-cover characteristic that exists. The multidimensional boundaries that separate the clusters are generally arbitrary and more a function of the number of classes the operator chooses rather than an identification of any real boundaries inherent in the image data. Clearly, successful image processing using standard image manipulations techniques is time consuming and expensive. As inexpensive image processing tools become more accessible to people not trained in traditional image processing techniques, the need for simple-to-use processes that return useful results becomes increasingly urgent.

In the traditional approach, the first step is to adjust the data for each of the three SPOT satellite bands to compensate for solar irradiance, sensor spectral band location, band width, and varying zenith angle of the sun (Price 1987). This converts the raw sensor values to a common scale that represents surface reflectance. This operation can be performed with the following equation:

$$R_k = \frac{\pi L_k d^2}{ESUN_k \cos\theta} \quad [\text{Eq 10}]$$

where  $k$  = image band

$R$  = unitless effective at-satellite reflectance

$L$  = spectral radiance defined as  $W/(m^2sr\mu m)$ , in which

$W$  = watts

$sr$  = solar, and

$\mu m$  = micrometers in light band

$$\begin{aligned}d &= \text{Earth to Sun distance in Astronomical Units} \\ESUN_k &= \text{mean solar exoatmospheric irradiance defined as } W/(m^2\mu m) \\ \theta_s &= \text{solar zenith angle, and} \\ \pi &= 3.1415926.\end{aligned}$$

The next step is to adjust these computed reflectance values to compensate for atmospheric conditions. Because actual atmospheric conditions were not explicitly known, this involved calibrating the images using pixels that have a known actual reflectance; in this case, pixels that represented a runway. The smallest values in each of the three bands found across a series of images of the same location are assumed to be most correct. All image bands then get proportionally adjusted to compensate. This procedure is based on Lo, Scarpace, and Lillesand (1986).

The third step is to calculate the normalized difference vegetation index (NDVI). This index is likely to have a strong correlation with the percent land cover values measured in the ground-truth procedure. The calculation involves subtracting the red band value from the near infrared value and dividing the result by the sum of these two values.

Finally, the NDVI values computed for each transect were regressed against the measured percent land cover values. Using all 89 transects, only a very poor correlation was discovered. After hypothesizing that the NDVI works best in grasslands, the regression was performed only for transects that did not contain forested areas. The resulting equations were applied to every pixel in the entire image to generate images showing derived percent land cover.

The neural network approach to correlating SPOT satellite imagery with percent land cover data collected on random transects compares very favorably with an approach based in image processing theory. Figure 27 shows measured percent land cover data (plotted on the x axis) versus percent land cover data modeled with the theory-based approach (using all transects) in graph a, using only non-forested transects in graph b, and the neural network in graph c. Compare graphs a and c with graph b and notice that graph b, the neural net modeled data, is more compact. Table 2 provides a comparison of the regressions of the measured data and several model inputs and outputs. Bands 1 through 3 represent the raw band data; note that there is some degree of natural correlation between the measured data and the raw satellite imagery. The theoretical-based models perform well. Figure 27 (d) shows that the neural network provides a network nearly identical to that generated based on theory; the last entry in Table 2 ( $R^2=.9955$ ) further demonstrates this fact.

Table 2

## Linear Regression Values for Comparing Model Predictability

Regression Between	R <sup>2</sup>
Image band 1 - LCTA measured %land cover	0.7954
Image band 2 - LCTA measured %land cover	0.6546
Image band 3 - LCTA measured %land cover	0.8585
Theoretical model with forest - LCTA measured %land cover	0.9652
Theoretical model w/o forest - LCTA measured %land cover	0.9686
Neural network model - LCTA measured %land cover	0.9851
Neural network model - Theoretical model w/forests %land cover	0.9955

Note: The neural network model trained the whole 90 data sets.

In another aspect, not only does the neural network emulate the theoretically-based model, but it also proves adaptable for simultaneously modeling the forested lands. Note that the forest data [represented by the data furthest to the right in Figures 27 (a) and (c)] falls closer to the regression line in the neural net model [Figure 27 (b)].

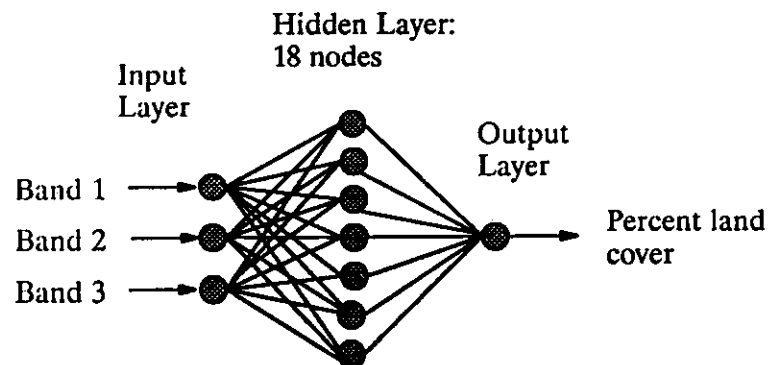
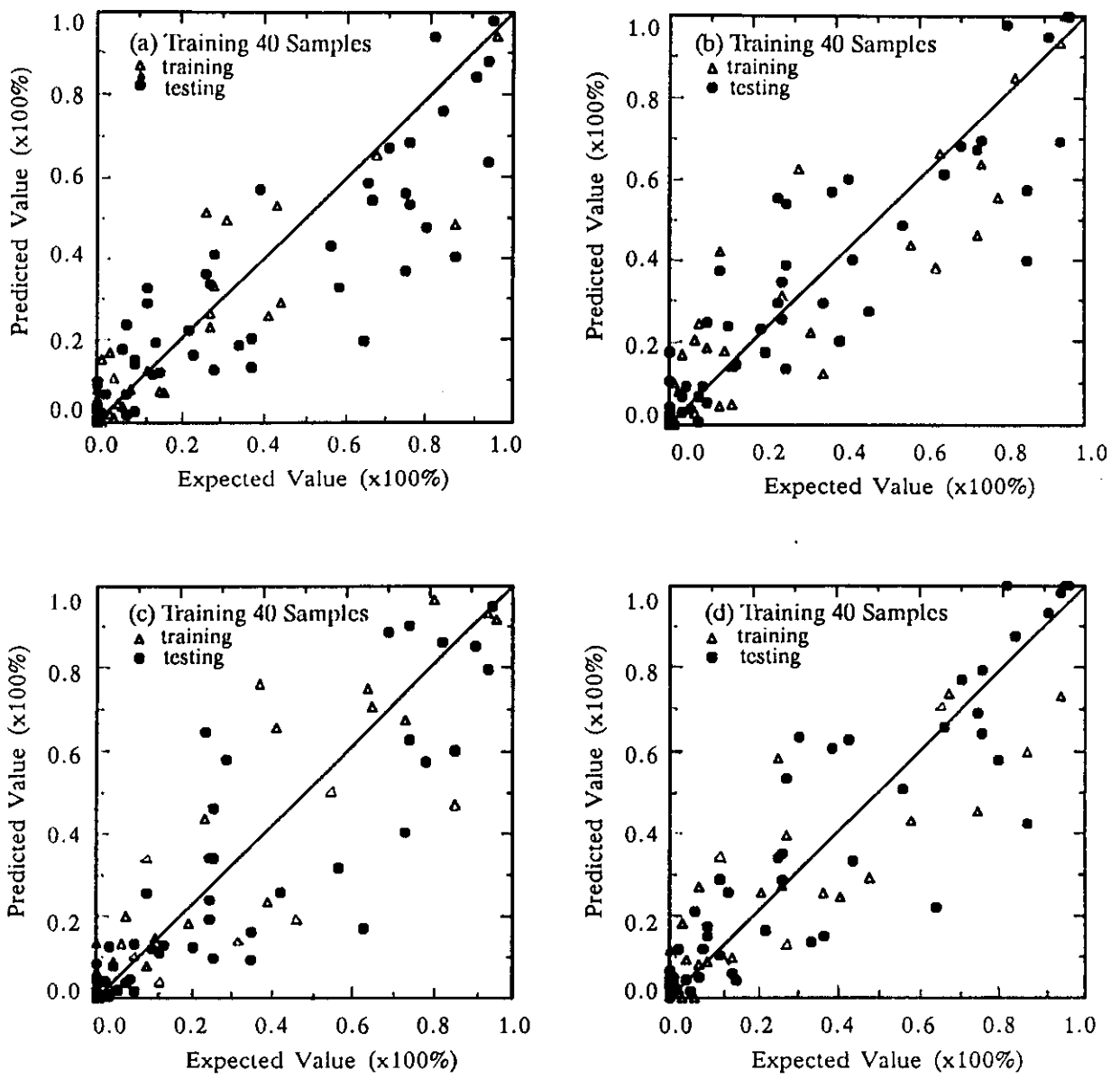
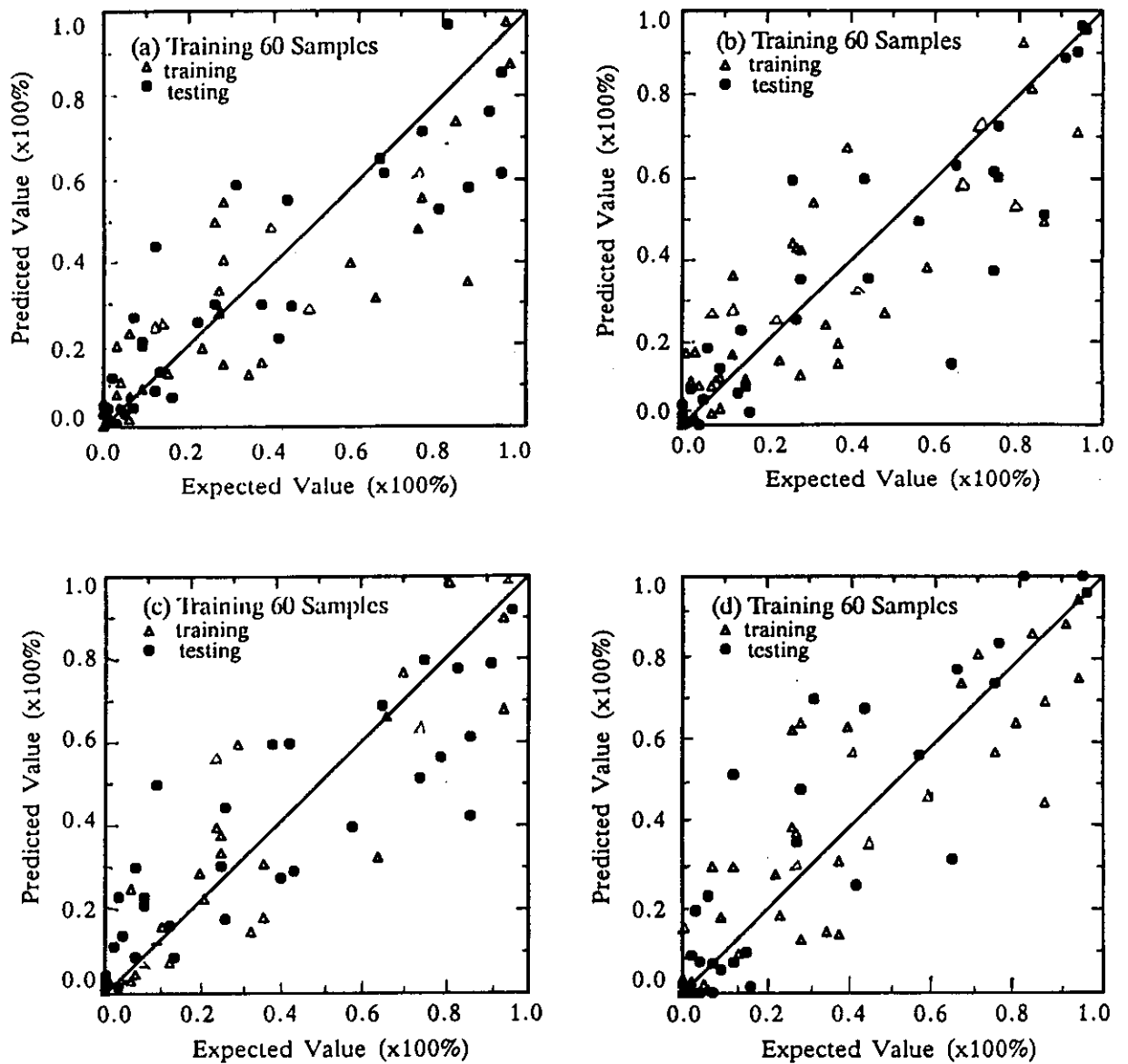


Figure 3. Architecture of the Neural Network for Percent Land Coverage Prediction.



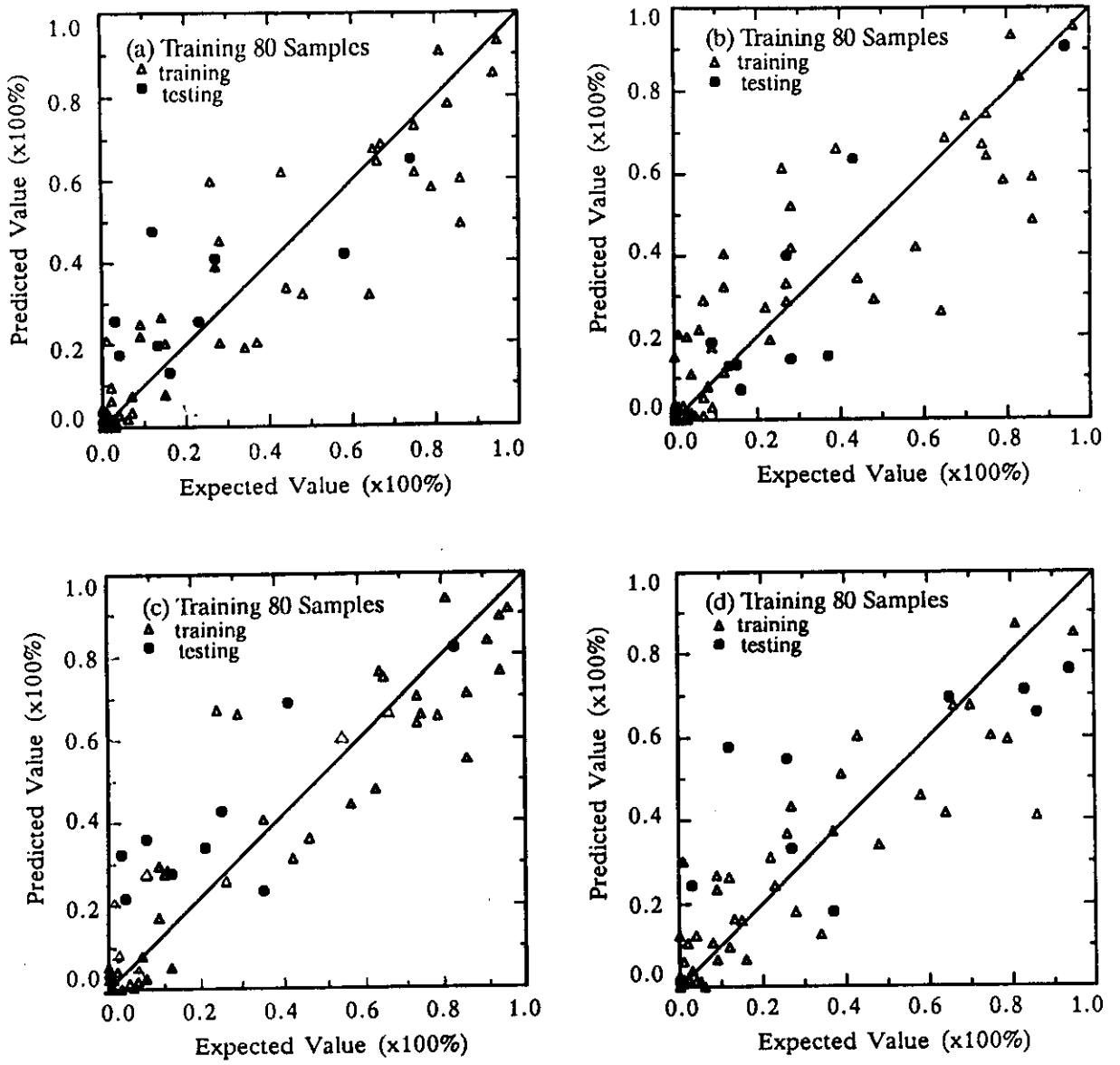
Sampling Batch No.	R <sup>2</sup>
(a)	0.8839
(b)	0.9039
(c)	0.9086
(d)	0.9007

Figure 4. Prediction of Percent of Land Cover (%LC) From the Neural Network With 40 Training Data Sets.



Sampling Batch No.	$R^2$
(a)	0.9026
(b)	0.8888
(c)	0.8998
(d)	0.8955

Figure 5. Prediction of Percent of Land Cover (%LC) From the Neural Network With 60 Training Data Sets.



Sampling Batch No.	R <sup>2</sup>
(a)	0.9325
(b)	0.8855
(c)	0.9153
(d)	0.9221

Figure 6. Prediction of Percent of Land Cover (%LC) From the Neural Network With 80 Training Data Sets.

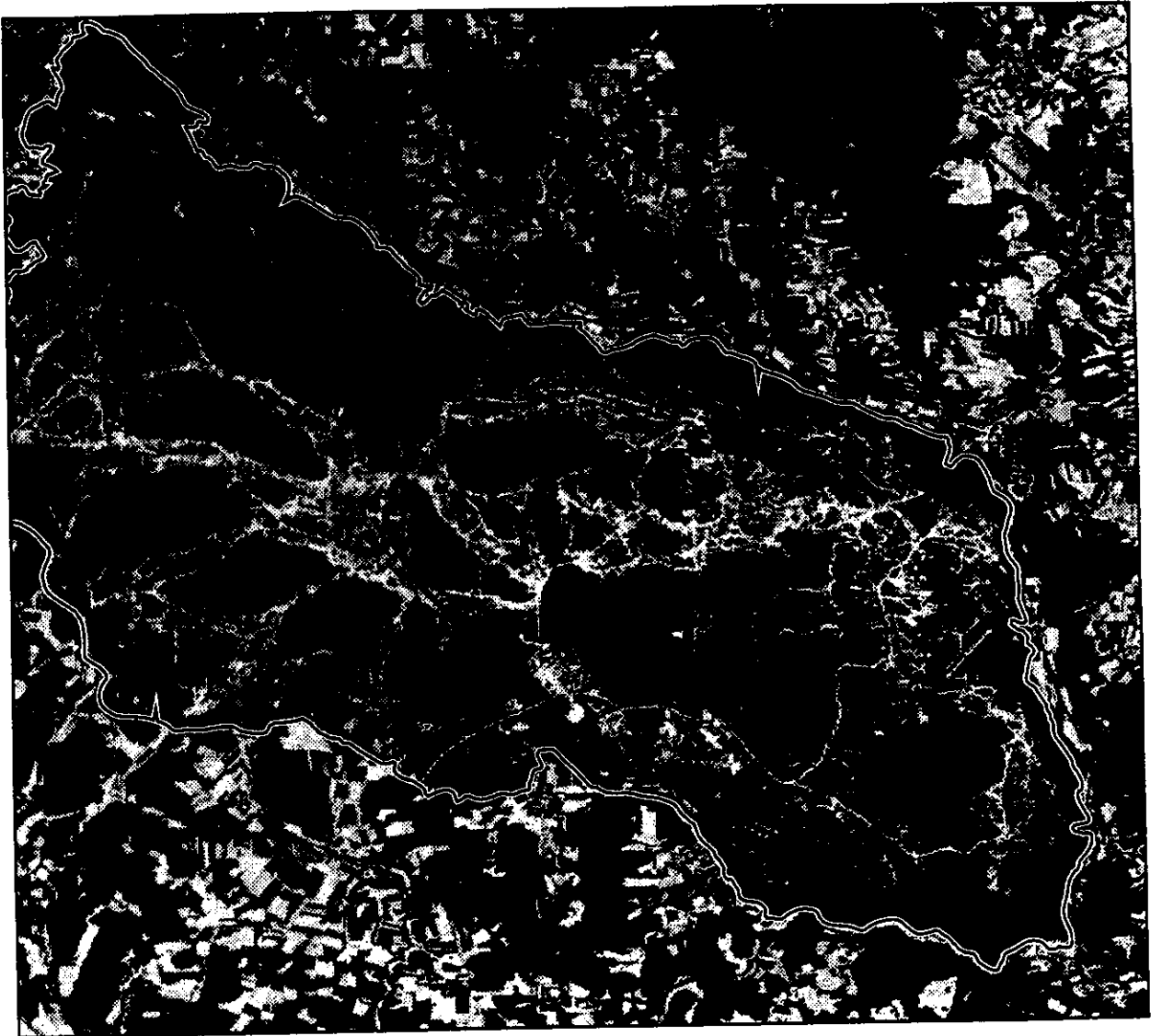
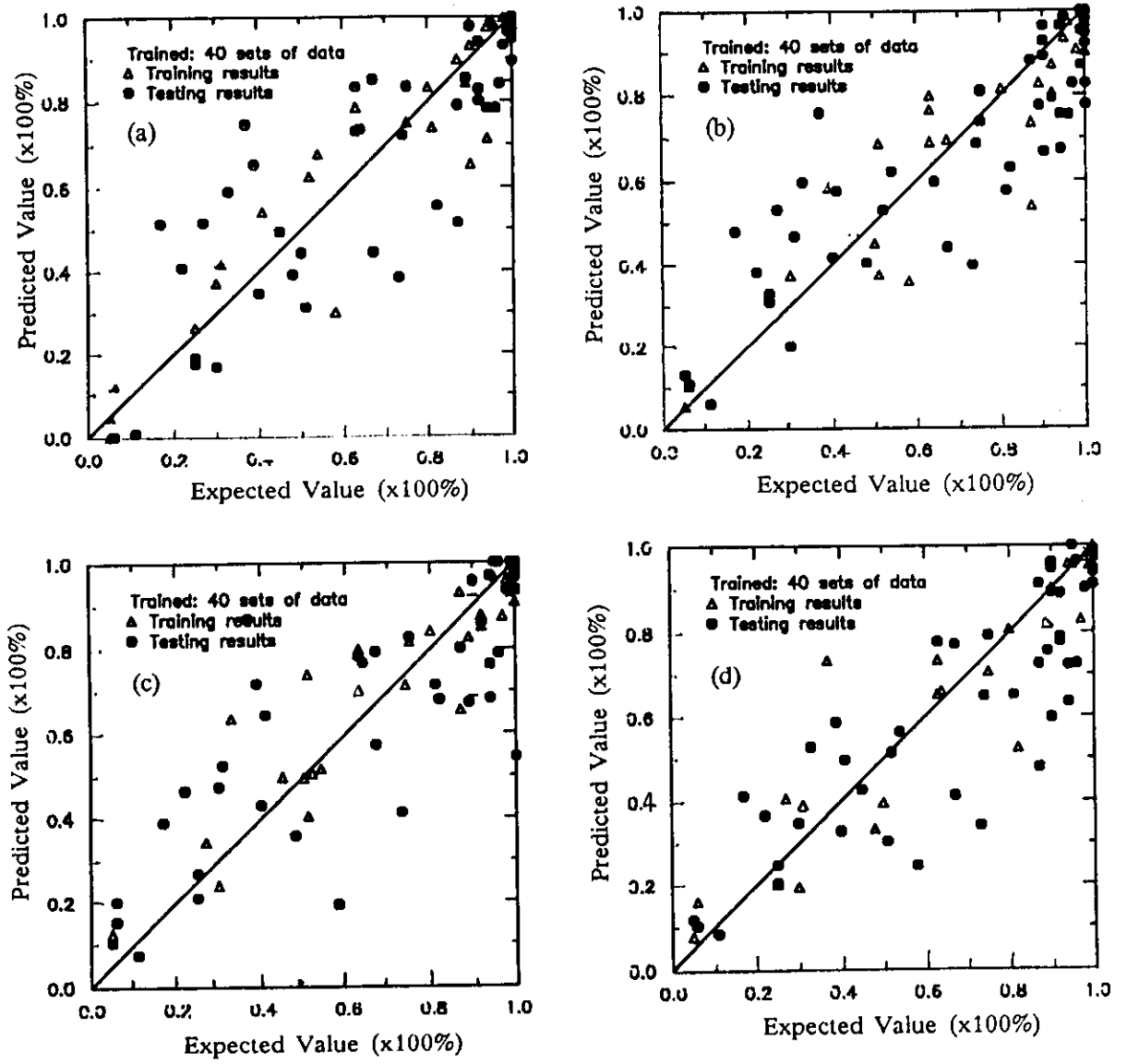
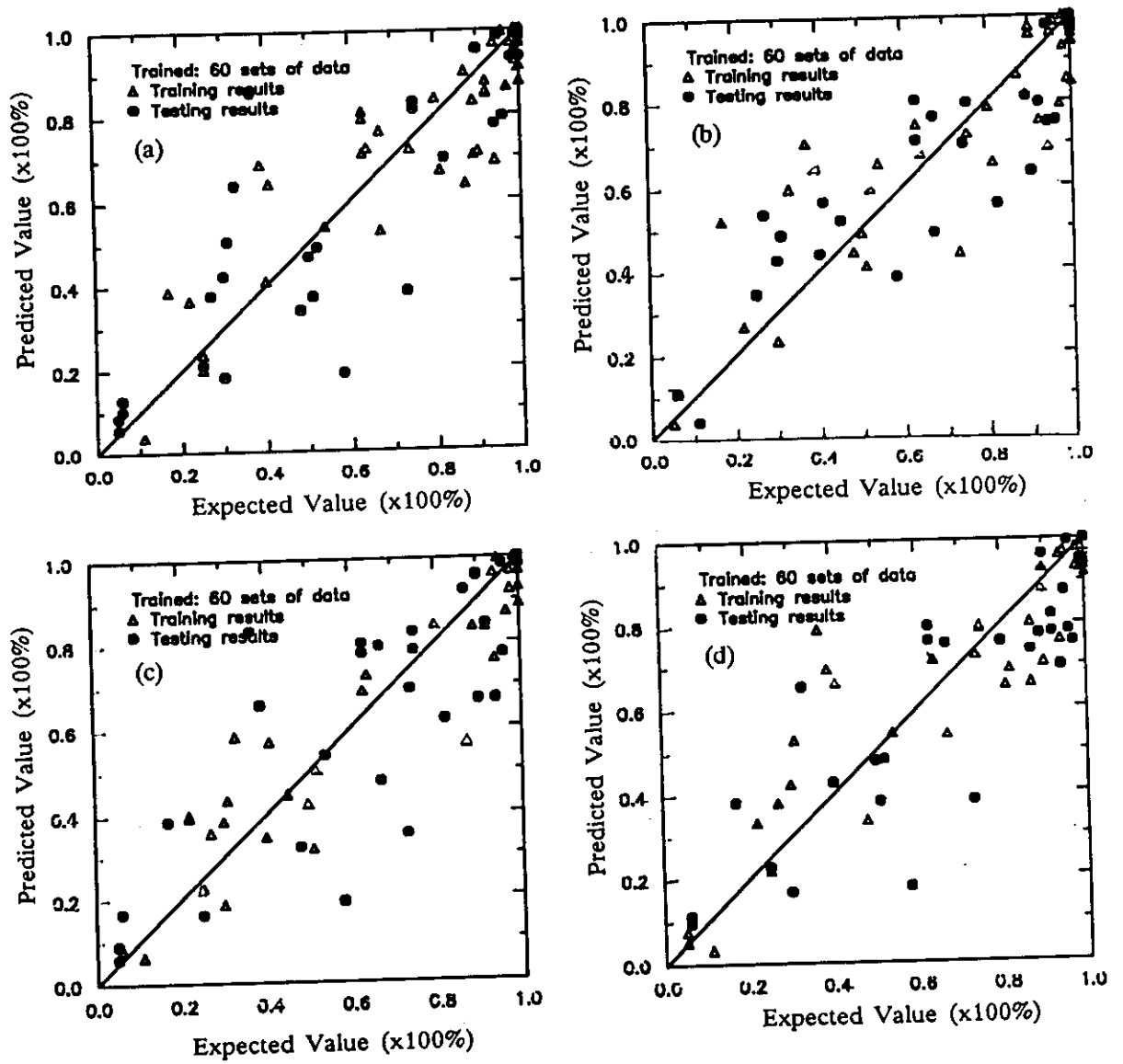


Figure 7. The Map of Percent of Land Cover (%LC) Predicted by the Neural Network.



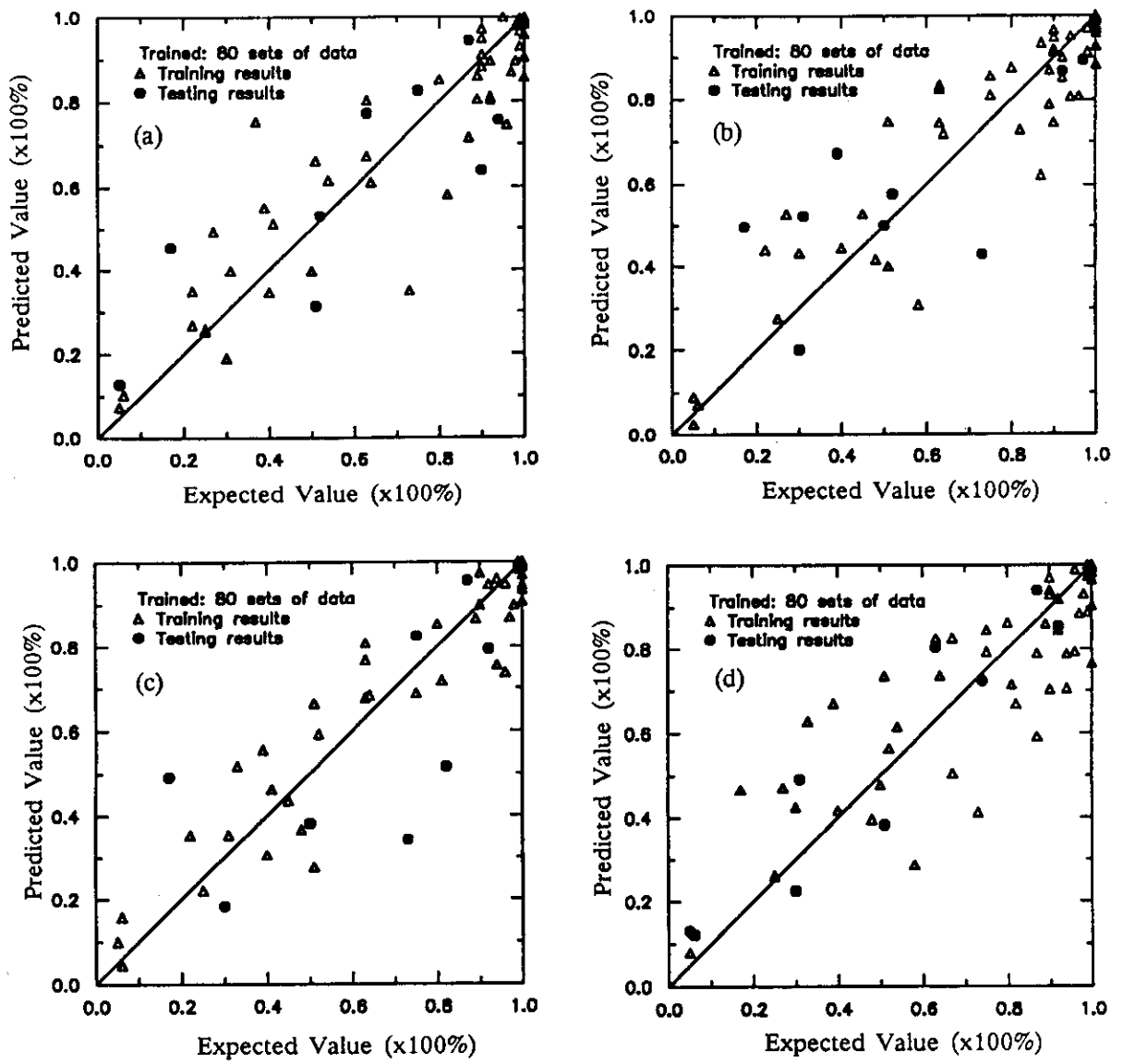
Sampling Batch No.	R <sup>2</sup>
(a)	0.8963
(b)	0.8927
(c)	0.8964
(d)	0.8900

Figure 8. Prediction of Percent of Bare Ground (%BG) From the Neural Network With 40 Training Data Sets.



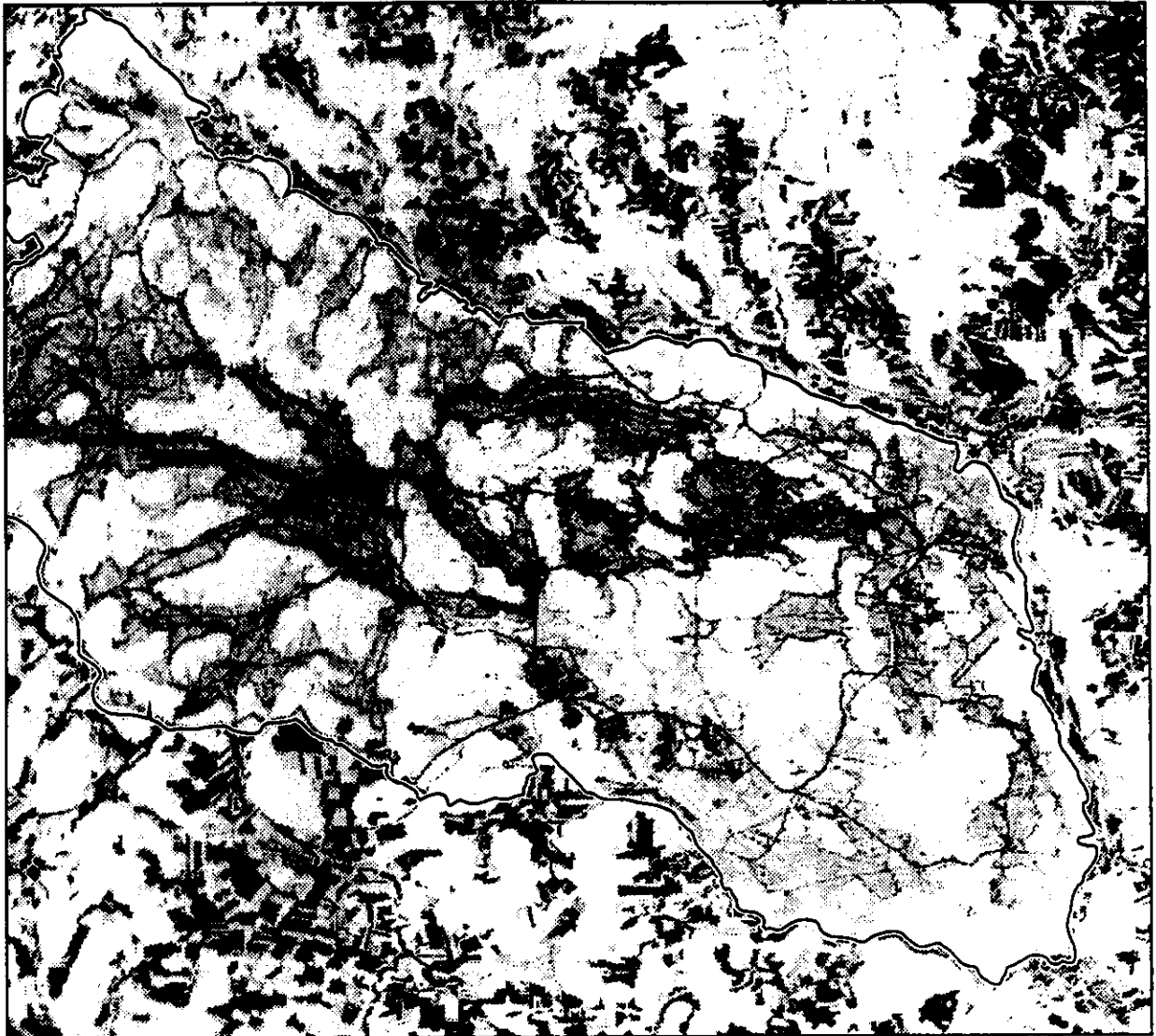
Sampling Batch No.	$R^2$
(a)	0.8590
(b)	0.8832
(c)	0.9067
(d)	0.8974

Figure 9. Prediction of Percent of Bare Ground (%BG) From the Neural Network With 60 Training Data Sets.

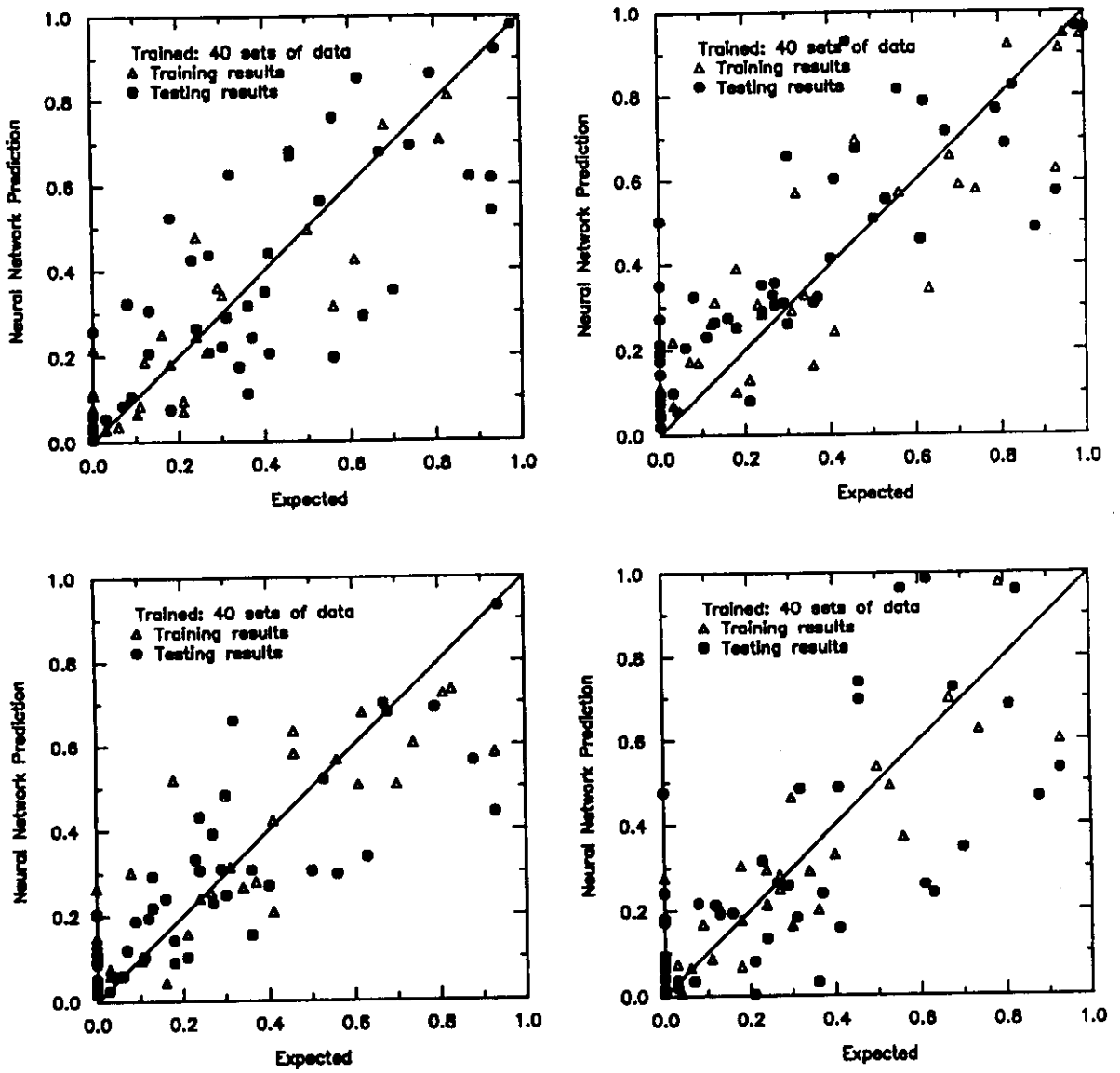


Sampling Batch No.	R <sup>2</sup>
(a)	0.9155
(b)	0.9156
(c)	0.8919
(d)	0.8866

Figure 10. Prediction of Percent of Bare Ground (%BG) From the Neural Network With 80 Training Data Sets.

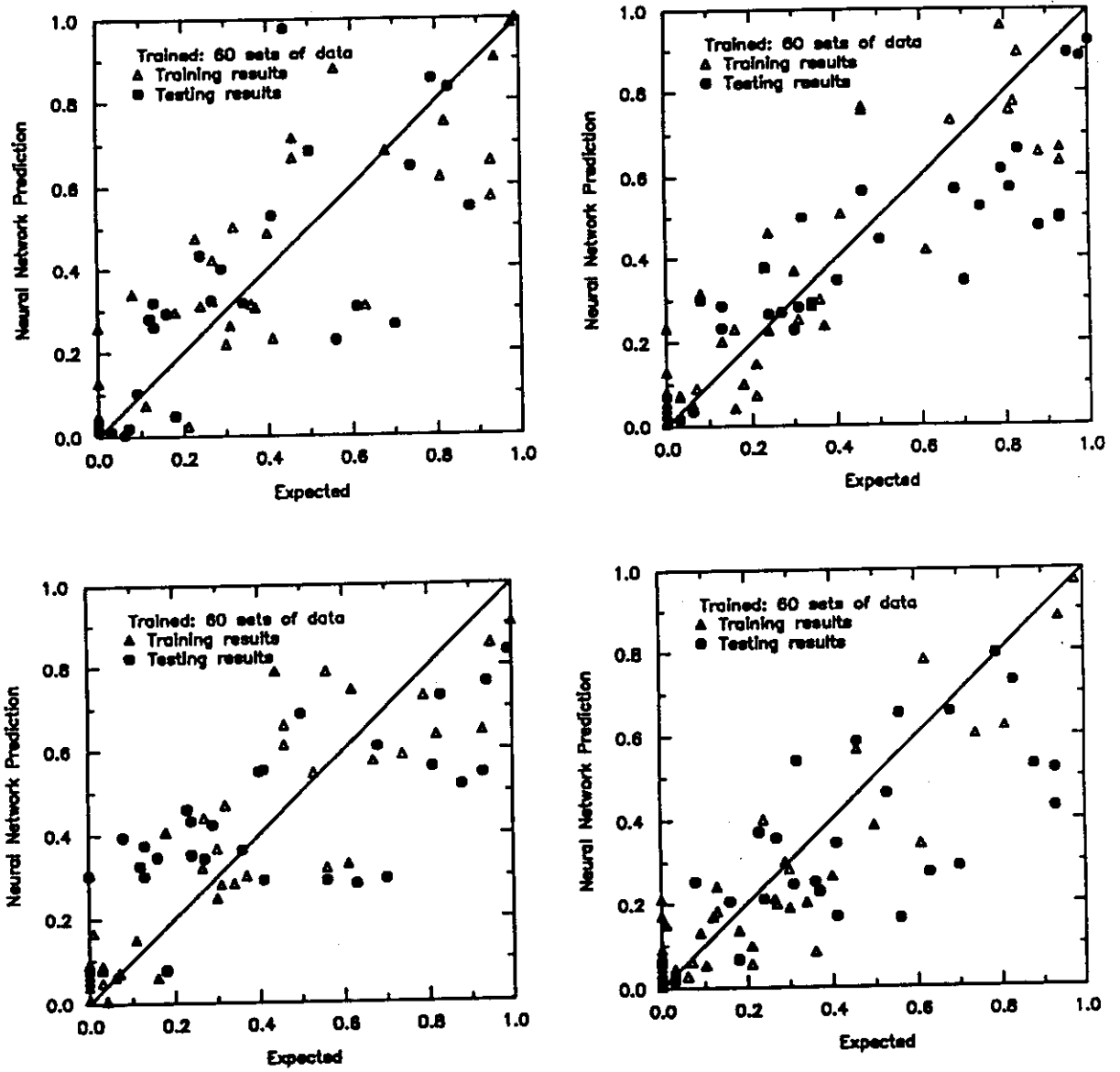


**Figure 11. The Map of Percent of Bare Ground (%BG) Predicted by the Neural Network.**



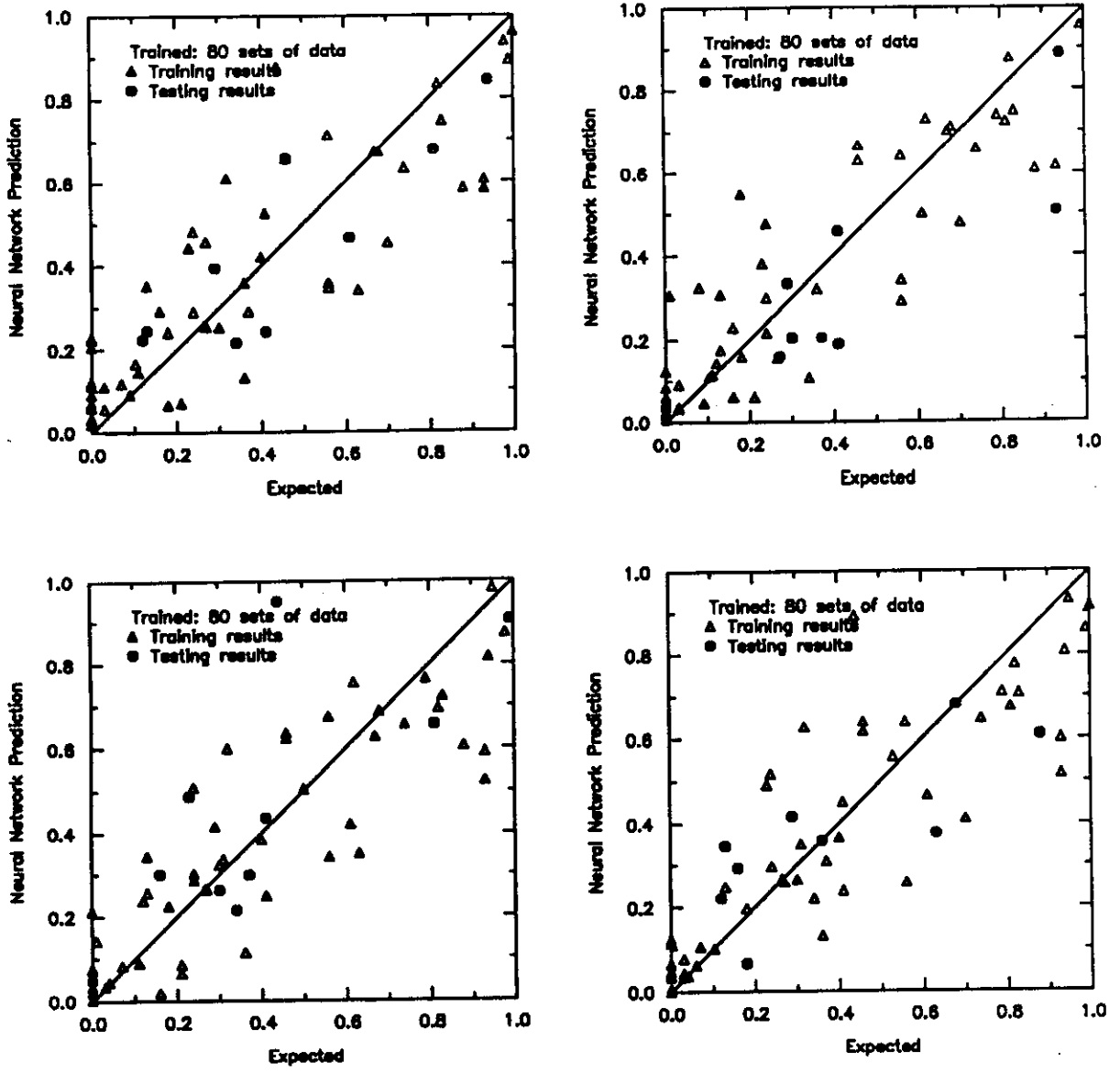
Sampling Batch No.	R <sup>2</sup>
(a)	0.8620
(b)	0.8316
(c)	0.8534
(d)	0.8451

Figure 12. Prediction of Percent Disturbance (%DIST) From the Neural Network With 40 Training Data Sets.



Sampling Batch No.	R <sup>2</sup>
(a)	0.8600
(b)	0.8767
(c)	0.8516
(d)	0.8897

Figure 13. Prediction of Percent Disturbance (%DIST) From the Neural Network With 60 Training Data Sets.



Sampling Batch No.	R <sup>2</sup>
(a)	0.8624
(b)	0.8793
(c)	0.8498
(d)	0.8746

Figure 14. Prediction of Percent Disturbance (%DIST) From the Neural Network With 80 Training Data Sets.



**Figure 15.** The Map of Percent Disturbance (%DIST) Predicted From the Neural Network With 60 Training Data Sets.

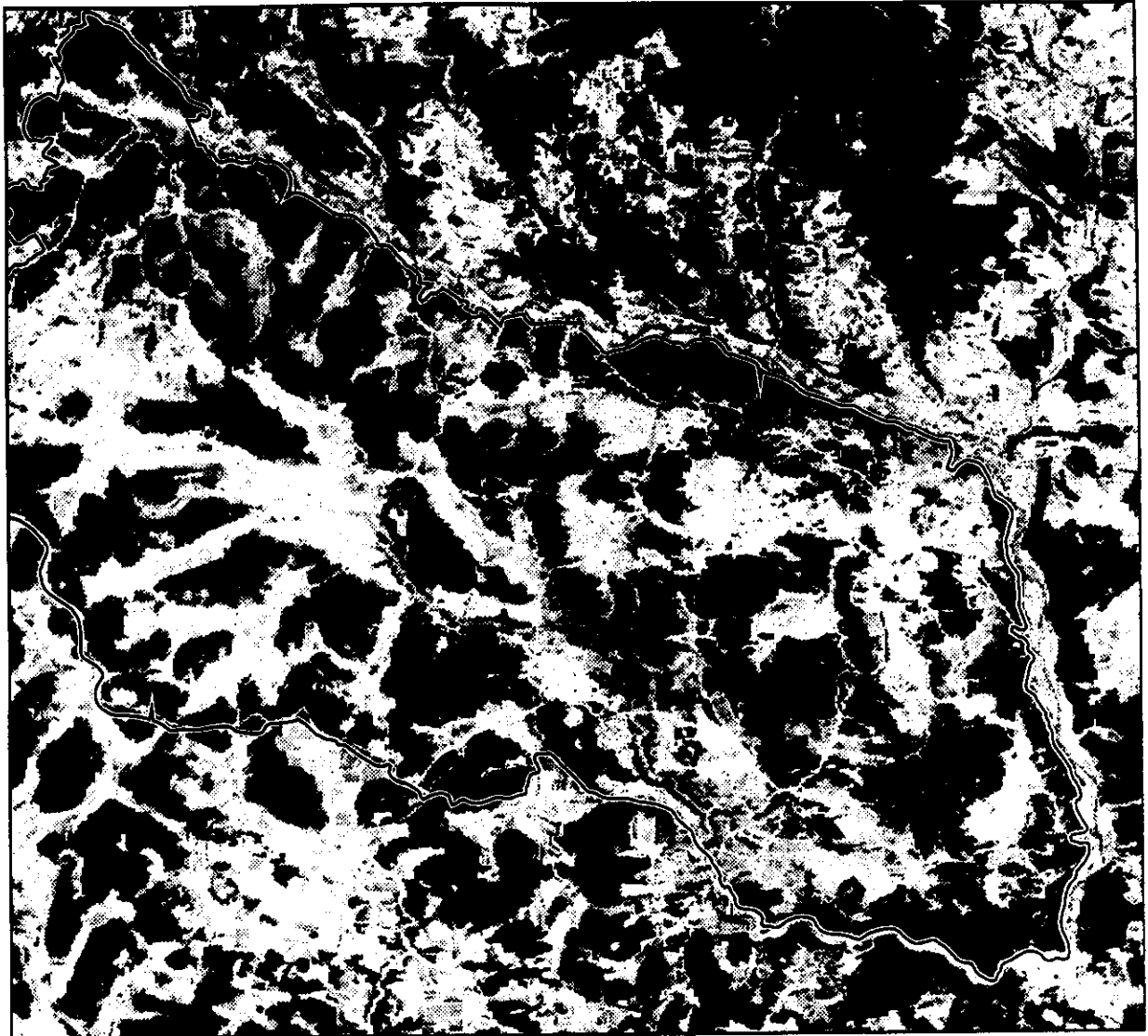


**Figure 16. The Map of Forest Presence Predicted by the Neural Network.**

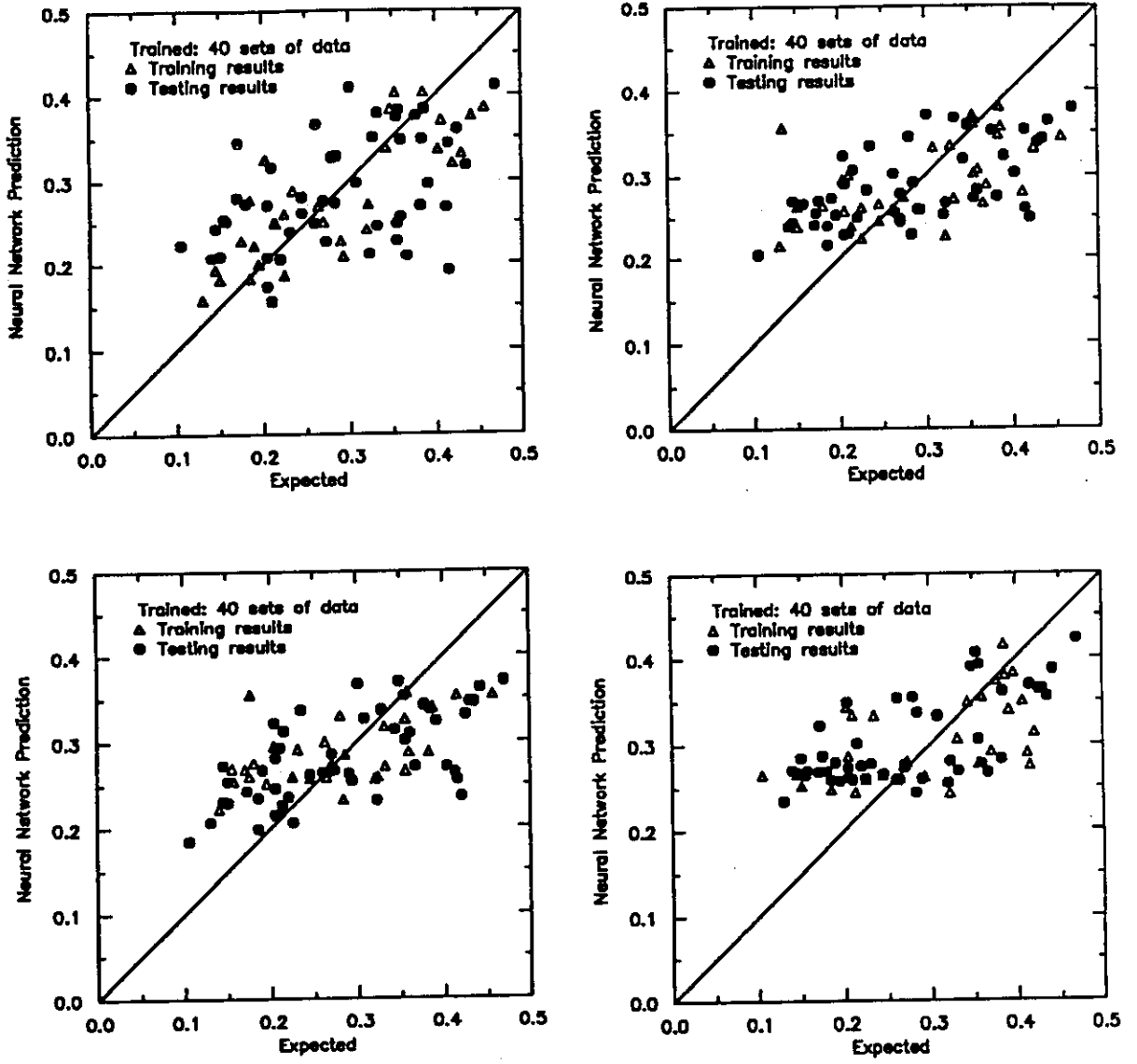


Figure 17. Prediction of Percent Clay (%CLAY) From the Neural Network With 40 Training Data Sets.

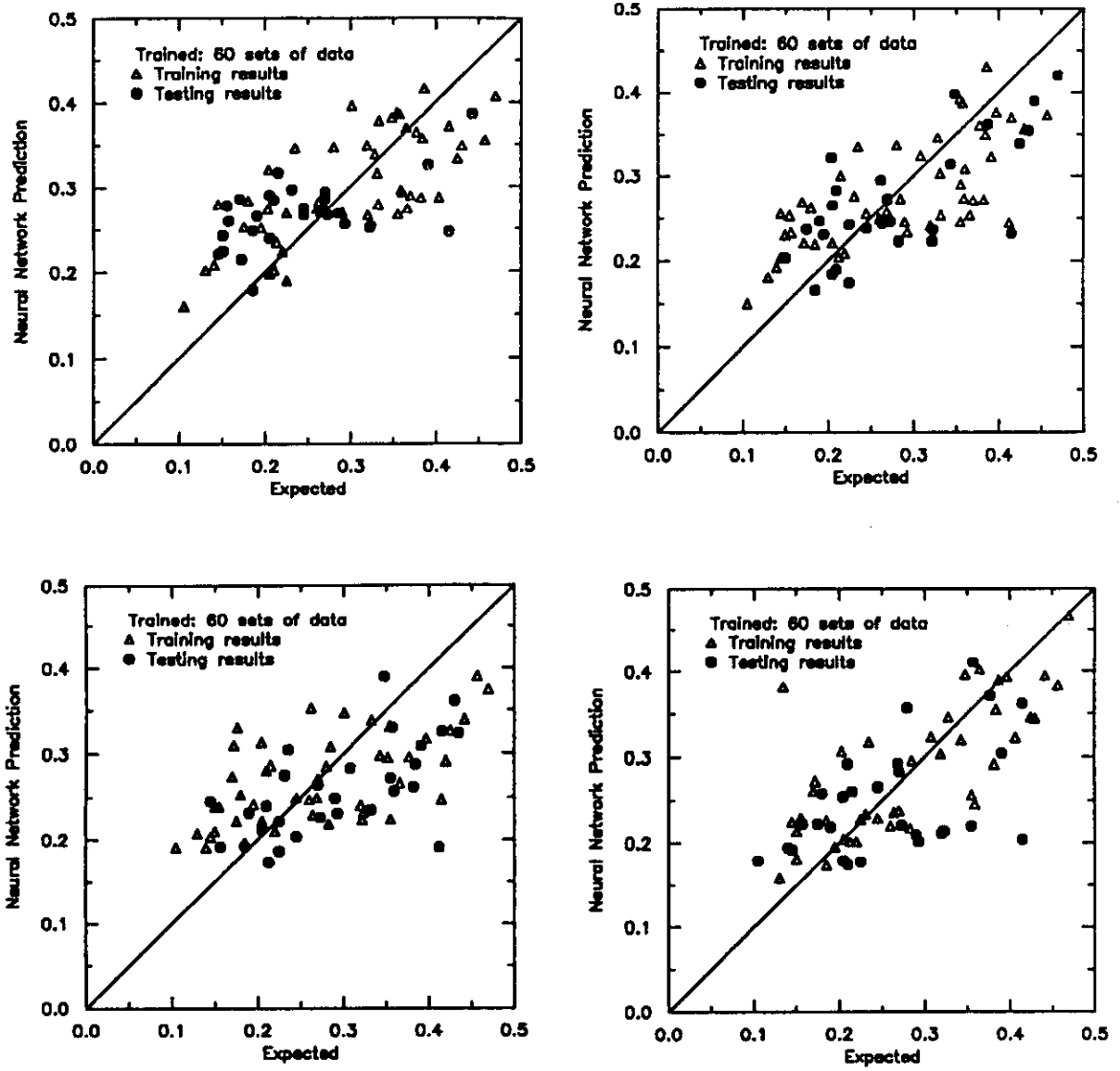


Figure 18. Prediction of Percent Clay (%CLAY) From the Neural Network With 60 Training Data Sets.

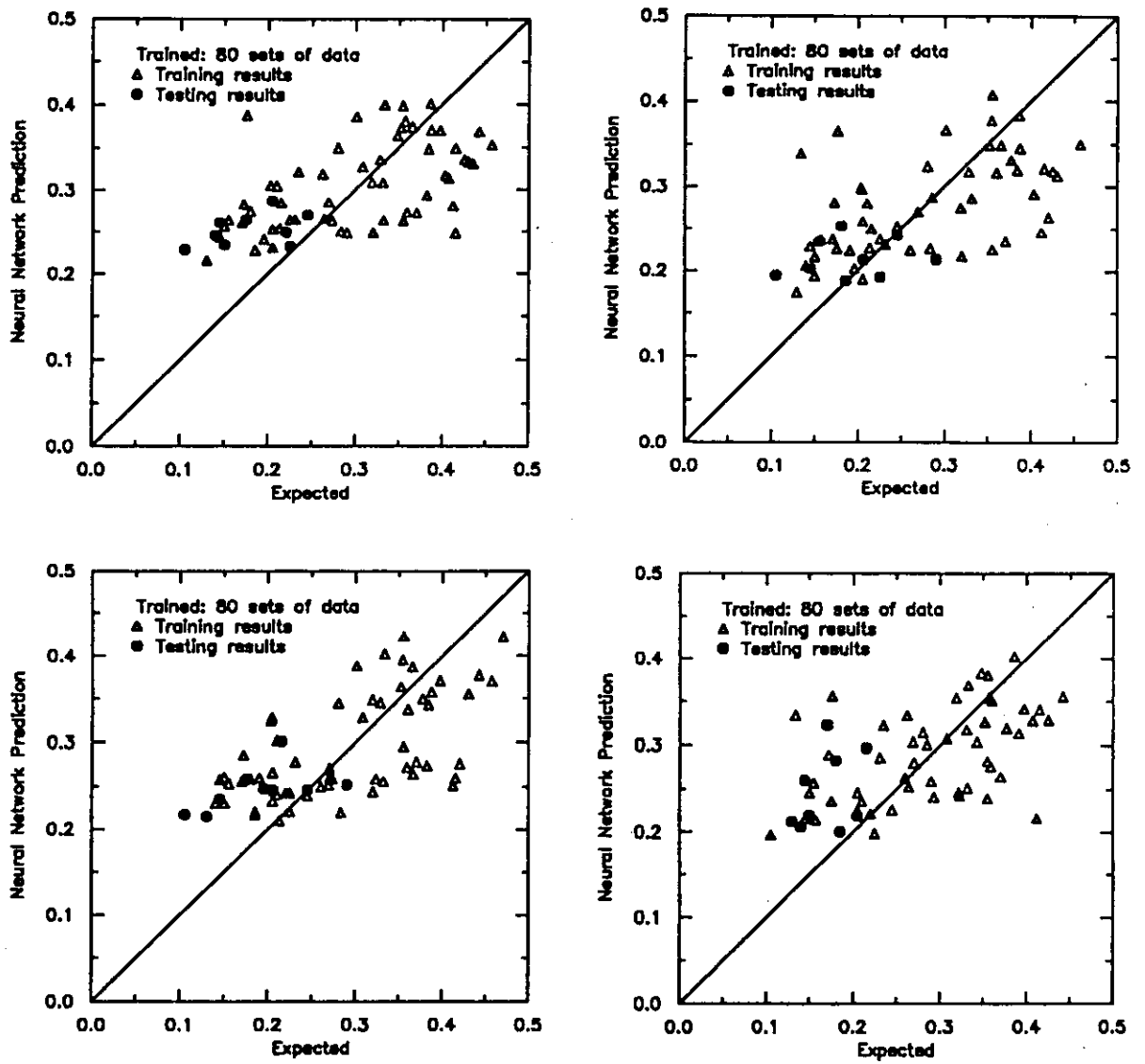


Figure 19. Prediction of Percent Clay (%CLAY) From the Neural Network With 80 Training Data Sets.

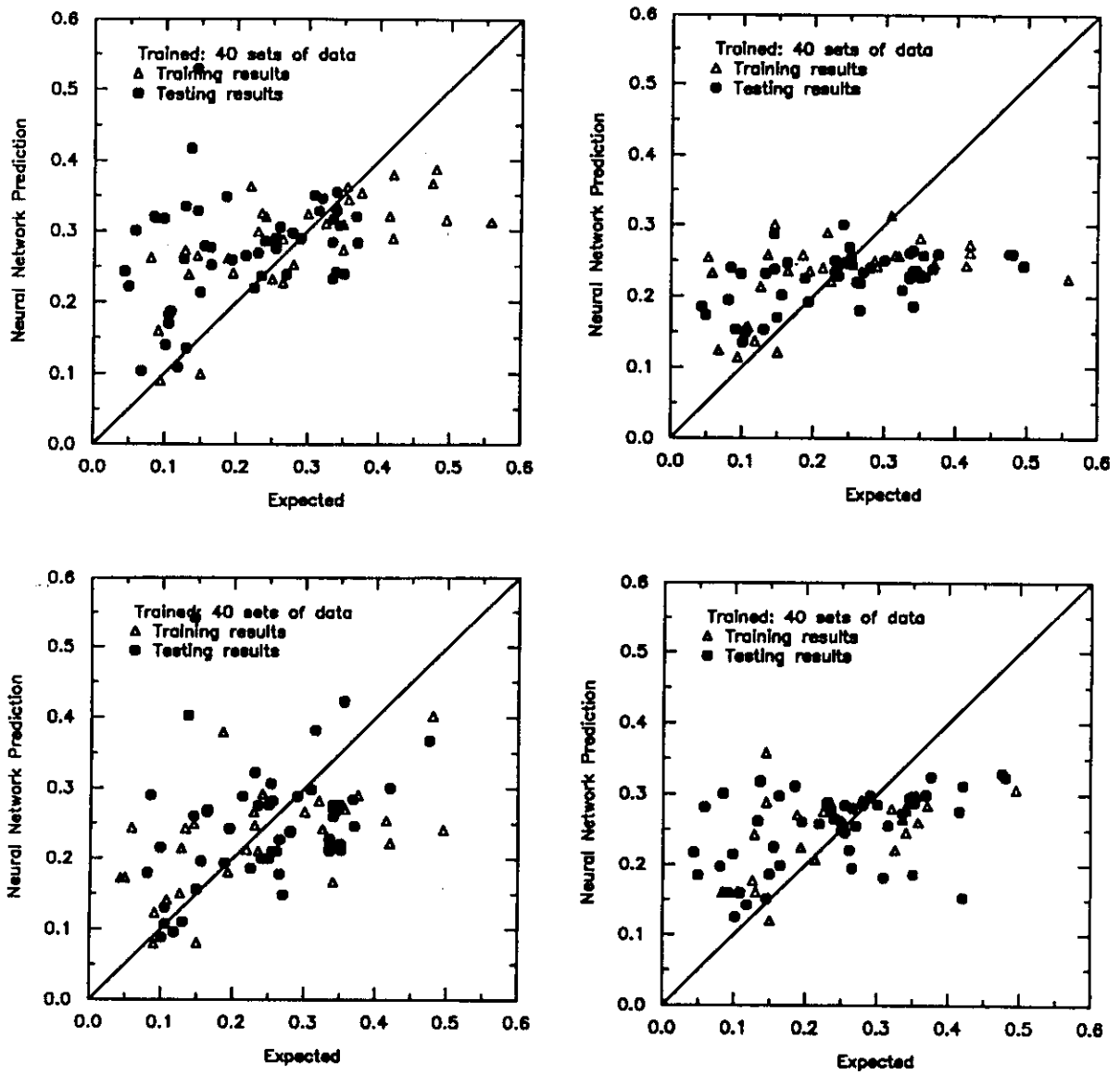


Figure 20. Prediction of Percent Sand (%SAND) From the Neural network With 40 Training Data Sets.

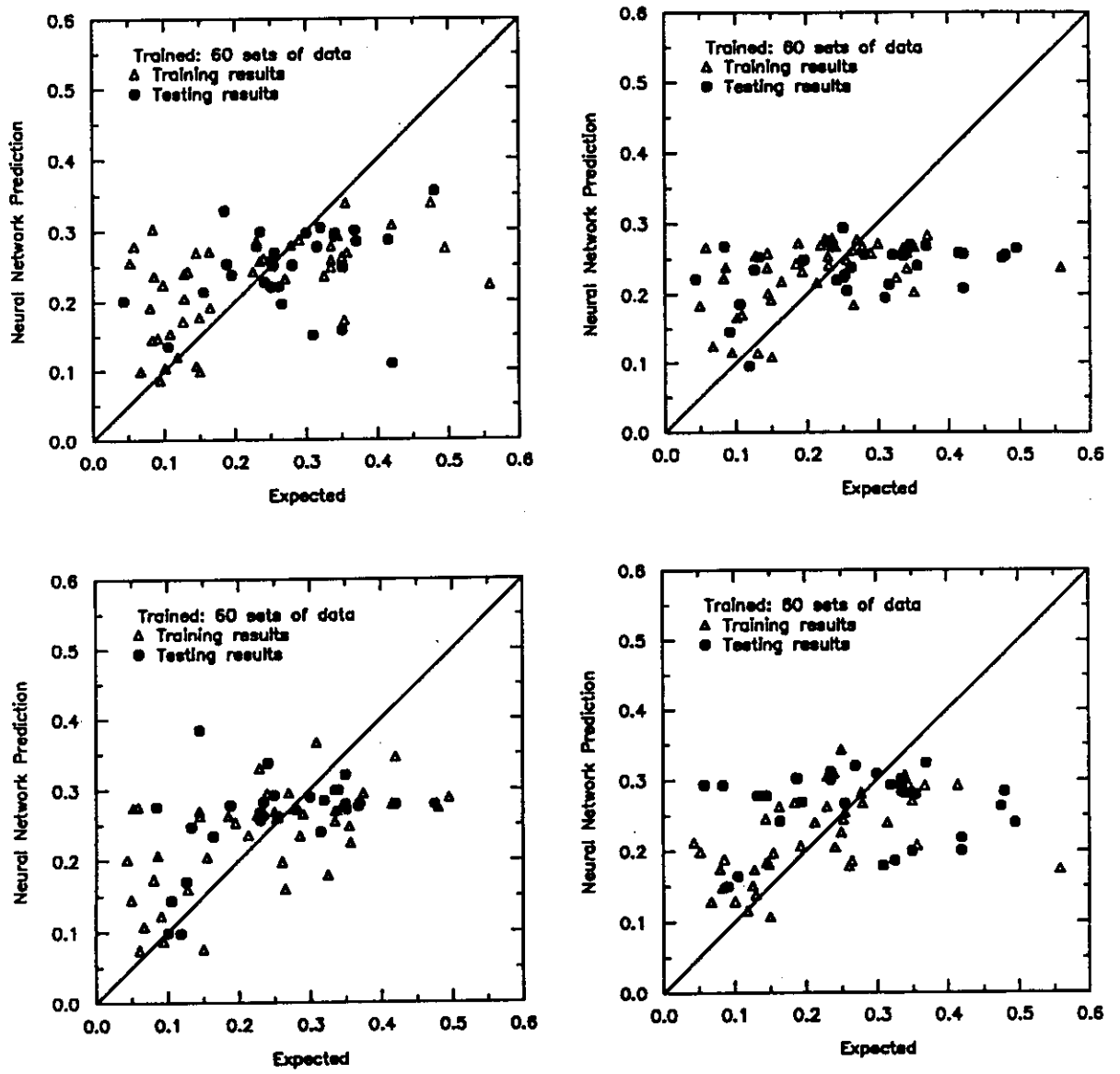


Figure 21. Prediction of Percent Sand (%SAND) From the Neural Network With 60 Training Data Sets.

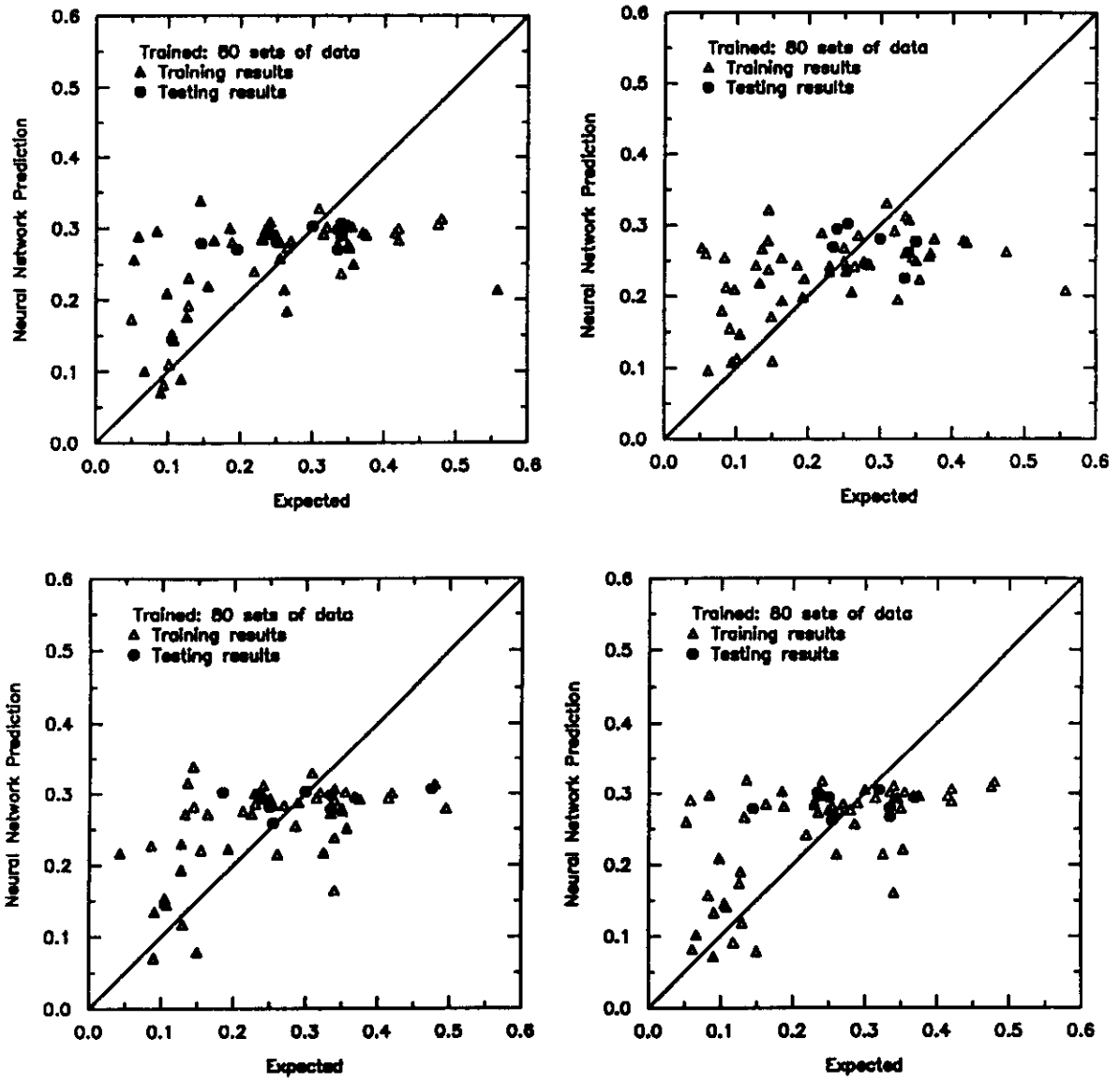


Figure 22. Prediction of Percent Sand (%SAND) From the Neural Network With 80 Training Data Sets.

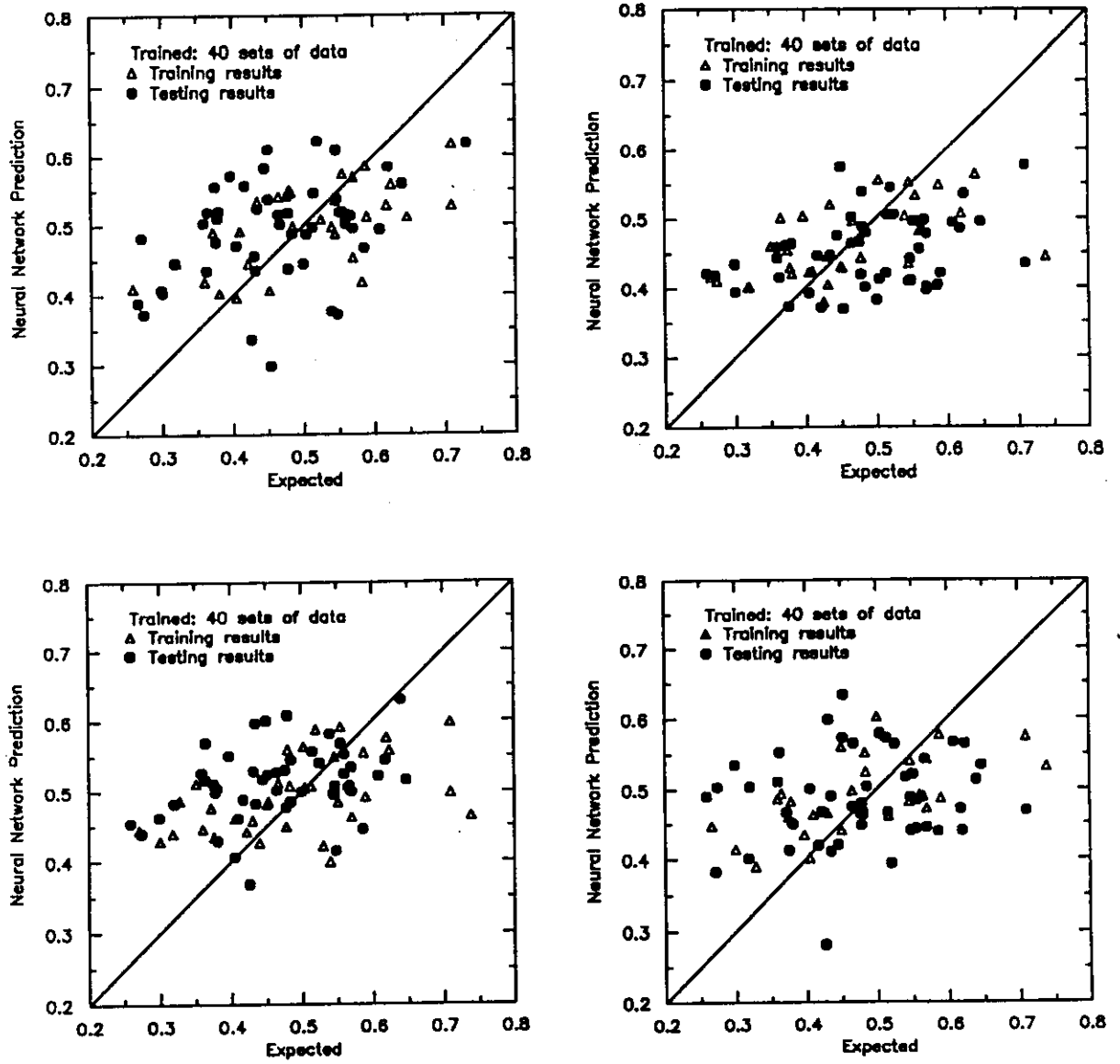


Figure 23. Prediction of Percent Silt (%SILT) From the Neural Network With 40 Training Data Sets.

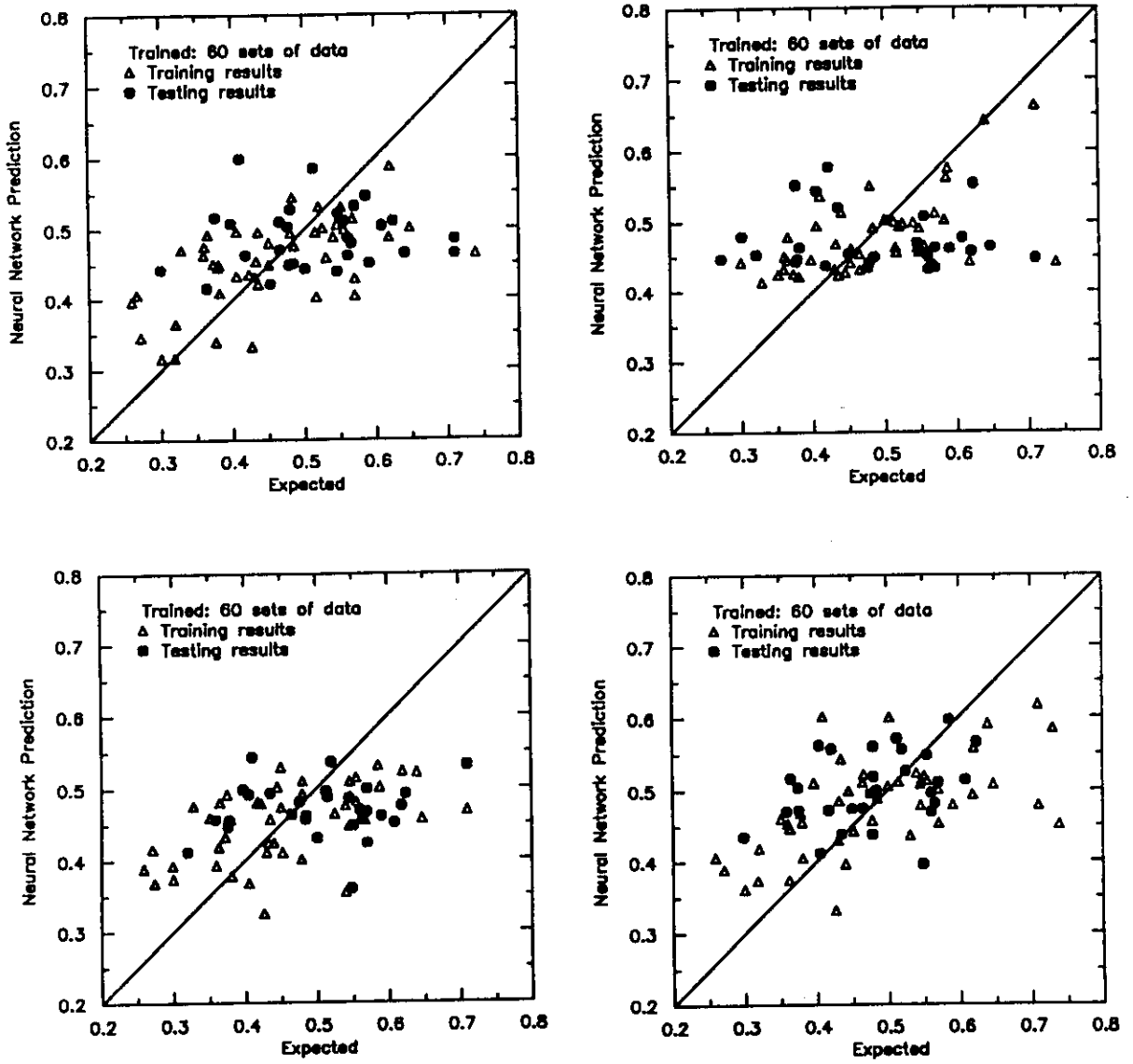


Figure 24. Prediction of Percent Silt (%SILT) From the Neural Network With 60 Training Data Sets.

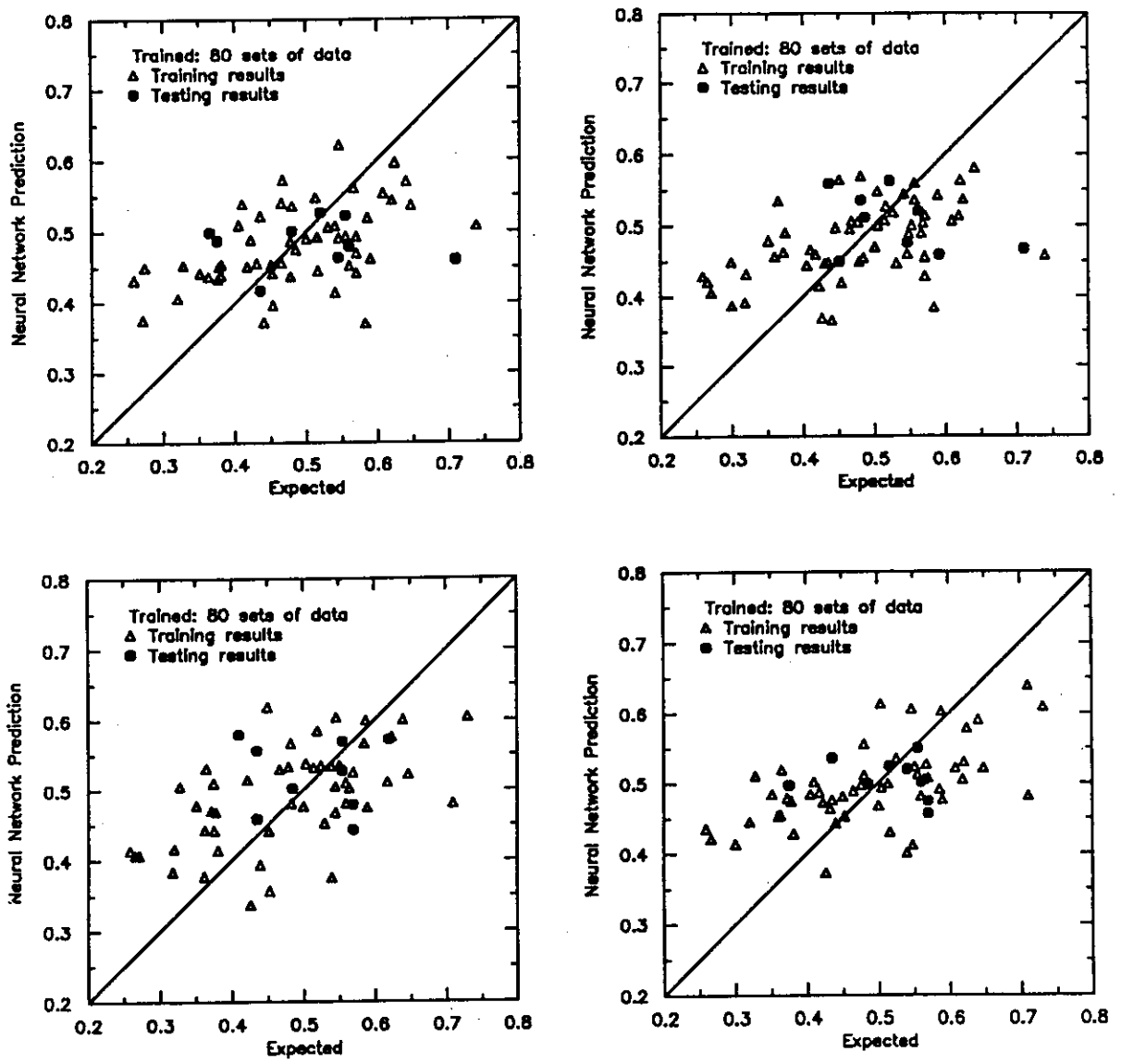


Figure 25. Prediction of Percent Silt (%SILT) From the Neural network With 80 Training Data Sets.



**Figure 26. The Map of Percent Clay Predicted by the Neural Network.**

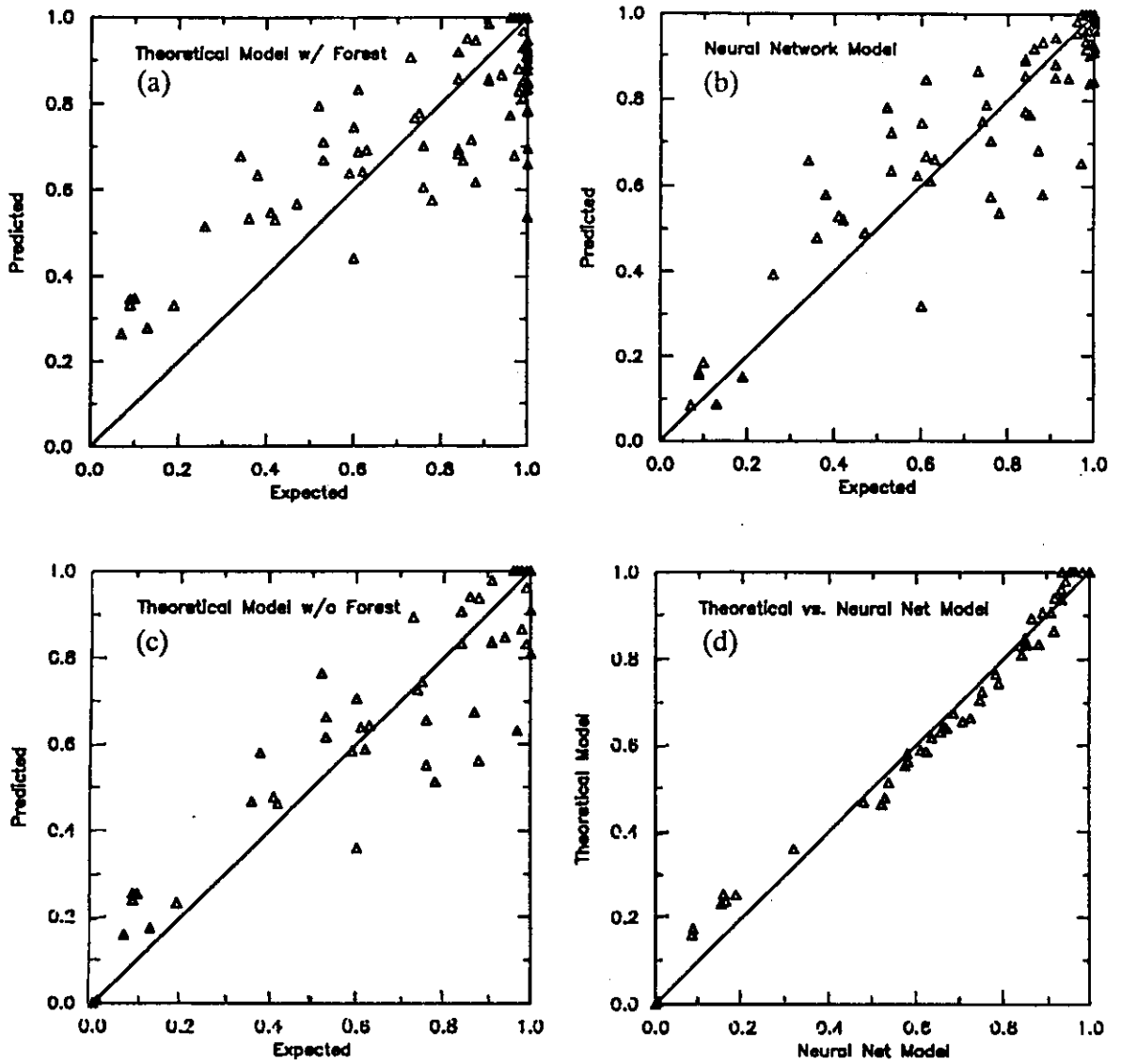


Figure 27. Comparison of Theoretical and Neural Network Results for Percent Land Cover.

## 4 CONCLUSIONS AND RECOMMENDATIONS

The neural network is very applicable for correlating satellite imagery and ground-truth data and performs better than the theoretical approach in several areas. Most important is that the operator's level of expertise in pursuing the neural network approach is far less than that required by the theoretical approach. This work was motivated by requirements to support such a user community; a group of trained scientists (ecologists, land managers, and foresters) working in an operational rather than academic environment.

A neural network-based GIS program can be used to attempt correlations between imagery data and other measured land cover information. The correlators constructed for predicting percent bare ground and percent ground disturbance appear to be reasonable and have reasonable statistical measurement. However, it is obvious that the training and testing results of correlating information on the percent clay, sand, and silt were not satisfactory, which indicates that additional information other than the three bands of imagery is needed to fully capture the relationships for these transects. More likely is that imagery is unsuitable for soil particle analysis, particularly when plant cover and/or organic matter content is high.

From the results obtained in this initial stage of research, it can be expected that a neural network-based approach will be very effective, not only in the correlation of satellite imagery and ground-truth data, but also in solving certain suitable classification and estimation problems encountered in land planning and management. However, further research on both the theory and application of neural computing needs to be carried out to make this approach a practical and efficient modeling procedure.

The goal of future research should be to capture the neural network software into a GIS program in which the user will need to identify only the input imagery bands, a file containing the percent land cover data, and, optionally, a few neural network parameters. Currently, the training and testing of the neural network modeling process still require the modeler to have a fairly good knowledge of the theory of neural computing; a fully adaptive modeling process is yet to be realized. Extended research in the development of adaptive training algorithms, therefore,

becomes imperative to reduce the burden in training and determining the network architecture.

To take advantage of the sophisticated image process capability in GRASS, it is important to incorporate the neural network modeling tools within GRASS to form an integral package.

To construct a robust and reliable neural network-based correlator, training and testing with the ground-truth data and corresponding satellite imagery collected over a long period of time and during different seasons should be studied.

## REFERENCES

- Ash, T., *Dynamic Node Creation in Backpropagation Networks*, ICS Report 8901 (Institute for Cognitive Science, University of California, San Diego, La Jolla, February 1989).
- Carpenter, G.A., and S. Grossberg, "A Massively Parallel Architecture for a Self-Organizing Neural Pattern Recognition Machine," *Computer Vision, Graphics, and Image Processing*, vol 37 (1987), pp 54-115.
- Fahlman, S.E., "Faster-Learning Variations of Backpropagation: An Empirical Study," *Proceedings of the 1988 Connectionist Models Summer School* (Morgan Kaufmann Publishers, Inc., 1988).
- Gallant, A.R., and H. White, "There Exists a Neural Network That Does Not Make Avoidable Mistakes," *Proceedings of the IEEE International Conference on Neural Networks* (1988).
- Grossberg, S., "Adaptive Pattern Classification and Universal Recoding: Part 1. Parallel Development and Coding of Natural Features Detectors," *Biological Cybernetics*, vol 23 (1976), pp 121-134.
- Hecht-Nielsen, R., "Kolmogorov's Mapping Neural Network Existence Theorem," in *Proceedings of the IEEE International Conference on Neural Networks* (1987).
- Hinton, G.E., T.J. Sejnowski, and D.H. Ackley, *Boltzmann Machines: Constraint Satisfaction Networks That Learn*, Technical Report CMU-CS-84-110 (Department of Computer Science, Carnegie Mellon University, Pittsburgh, PA, 1984).
- Hopfield, J.J., "Neural Networks and Physical Systems with Emergent Collective Computational Abilities," *Proceeding of the National Academy of Sciences*, vol 79 (1982), pp 2554-2558.
- Hornik, K., M. Stinchcombe, and H. White, "Multilayer Feedforward Networks are Universal Approximators," *Neural Networks*, vol 2 (1989), pp 359-366.
- Jacobs, R.A., *Increased Rate of Convergence Through Learning Rate Adaptation*, Technical Report COINS TR 87-117 (Department of Computer and Information Science, University of Massachusetts at Amherst, MA, 1988).
- Jensen, J.R., *Introductory Digital Image Processing—A Remote Sensing Perspective* (Prentice Hall 1986).
- Judd, S., *Neural Network Design and the Complexity of Learning* (The MIT Press, 1990).
- Karnin, E.D., "A Simple Procedure for Pruning Backpropagation Trained Neural Networks," *IEEE Transactions on Neural Networks*, vol 1, no. 2 (June 1990), pp 239-242.

- Kohonen, T., G. Barna, and R. Chrisley, "Statistical Pattern Recognition With Neural Networks: Benchmarking Studies" in *Proceedings of the IEEE International Conference on Neural Networks* (1988), pp 61-68.
- Lillesand, T.M. and R.W. Kiefer, *Remote Sensing and Image Interpretation* (John Wiley and Sons, Inc., 1987).
- Lo, T., F. Scarpace, and T. Lillesand, "Use of Multitemporal Spectral Profiles in Agricultural Land-Cover Classification," *Photogrammetric Engineering and Remote Sensing*, vol 52, no. 4 (1986), pp 533-544.
- Price, J.C., "Calibration of Satellite Radiometers and the Comparison of Vegetation Indices," *Remote Sensing of the Environment*, vol 21 (1987), pp 15-27.
- Rumelhart, D., and D. Zipser, "Feature Discovery by Competitive Learning," *Cognitive Science*, vol 9 (1985), pp 75-112.
- Rumelhart, D.E., G.E. Hinton, and R.J. Williams, "Learning Internal Representations by Error Propagation," *Parallel Distributed Processing, Vol 1: Foundations* (The MIT Press, 1986).
- Tazik, David J. et al., USACERL Technical Report N-92/03/ADA247931. *U.S. Army Land Condition - Trend Analysis (LCTA) Plot Inventory Field Methods* (U.S. Army Construction Engineering Research Laboratories [USACERL], February 1992).
- Tenorio, M.F.M., and W.T. Lee, *Self-Organizing Neural Network for Optimum Supervised Learning*, Technical Report TR-EE-89-30 (School of Electrical Engineering, Purdue University, June 1989).
- Watrous, R.L., "Learning Algorithm for Connectionist Networks: Applied Gradient Methods of Nonlinear Optimization," *Proceedings of the IEEE International Conference on Neural Networks*, vol II (1987), pp 619-627.
- Wolpert, D.H., "A Mathematical Theory of Generalization," *Complex Systems*, vol 4 (1990), pp 151-249.
- Wu, X., *Neural Network-Based Material Modeling*, Ph.D. Thesis (Department of Civil Engineering, University of Illinois at Urbana-Champaign, 1991).

## USACERL DISTRIBUTION

## Chief of Engineers

ATTN: CEHEC-IM-LH (2)  
 ATTN: CEHEC-IM-LP (2)  
 ATTN: CERD-M  
 ATTN: CERD-L  
 ATTN: CECW  
 ATTN: CEMP  
 ATTN: CERD-C  
 ATTN: DAEN-ZCE

## CECPW

ATTN: CECPW-F 22060

## US Army Engr District

ATTN: Library  
 Mobile 36828  
 Detroit 48231  
 St Paul 55101  
 St Louis 63103  
 Omaha 68102  
 Fort Worth 76544  
 Galveston 77553  
 San Francisco 94105  
 Walla Walla 99362  
 Alaska 99506

## US Army Europe

CMTC Hohenfels 09173  
 ATTN: AETTH-DPW  
 21st Support Command  
 Zweibruecken 09052  
 ATTN: AERZE  
 Burtonwood England 09448  
 ATTN: AERUK-E  
 NATO/SHAPE 09708  
 ATTN: AERSH-EH

## Defense Distribution Region East

ATTN: DDRE-WI 17070

## US Army Materiel Command (AMC)

Redstone Arsenal 35809  
 ATTN: AMSMI-RA-EH  
 Dugway Proving Ground 84022  
 ATTN: STEDP-EN  
 Yuma Proving Ground 85365  
 ATTN: STEYP-EH  
 Red River Army Depot 75507  
 ATTN: SDSRR-G  
 White Sands Missile Range 88002  
 ATTN: STEWS-EL  
 Picatinny Arsenal  
 ATTN: SMCAR-ISE

## FORSCOM

Forts Gillem & McPherson 30330  
 ATTN: FCEN

## Installations:

## FHE

Fort McPherson 30330  
 ATTN: AFZK-EH  
 Fort Riley 66442  
 ATTN: AFZN-

## DE

Fort Polk 71459  
 ATTN: AFZX-DE  
 Fort Ord 93941  
 ATTN: AFZW-DE  
 Fort Lewis 98433  
 ATTN: AFZH-DE  
 Fort Carson 80913  
 ATTN: AFZC-FE  
 Fort Bragg 28307  
 ATTN: AFZA-DE  
 Fort Campbell 42223  
 ATTN: AFZB-DPW  
 Fort McCoy 54656  
 ATTN: AFZR-DE  
 Fort Stewart 31314  
 ATTN: AFZP-DE  
 Fort Drum 13602  
 ATTN: AFZS-EH  
 Fort Irwin 92310  
 ATTN: AFZJ-EH  
 Fort Hood 76544  
 ATTN: AFZF-DE

## TRADOC

Fort Monroe 23651  
 ATTN: ATBO-G  
 Installations:  
 Fort Dix 08640  
 ATTN: ATZD-EH  
 Fort Jackson 29207  
 ATTN: ATZJ-EH  
 Fort Gordon 30905  
 ATTN: ATZH-DI  
 Fort Benning 31905  
 ATTN: ATZB-EH  
 Fort McClellan 36205  
 ATTN: ATZN-FE  
 Fort Rucker 36362  
 ATTN: ATZQ-DPW  
 Fort Benjamin Harrison 46216  
 ATTN: ATZI-IS  
 Fort Leonard Wood 65473  
 ATTN: ATZT-DPW  
 Fort Bliss 79916  
 ATTN: ATZC-IS  
 Fort Chaffee 72905  
 ATTN: ATZR-ZF  
 Fort Sill 73503  
 ATTN: ATZR-E  
 Fort Huachuca 85613  
 ATTN: ATZS-EH  
 Fort Knox 40121  
 ATTN: ATZK-EH

## Fort Belvoir 22060

ATTN: CETEC-IM-T  
 ATTN: CECC-R 22060  
 ATTN: Engr Strategic Studies Ctr  
 ATTN: Water Resources Support Ctr  
 ATTN: Australian Liaison Office

## USA Natick RD&amp;E Center 01760

ATTN: STRNC-DT

## CEWES 39180

ATTN: Library

## CECRL 03755

ATTN: Library

## US Army ARDEC 07806

ATTN: SMCAR-ISE

## Engr Societies Library

ATTN: Acquisitions 10017

## National Guard Bureau 20310

ATTN: NGB-ARI

## US Military Academy 10996

ATTN: Geography & Envr Engrg

## Naval Facilities Engr Command

Pacific Division 96860  
 ATTN: Code 04B (2)

## 8th US Army Korea

2nd Infantry Division  
 ATTN: EAFE-ID

## Tyndall AFB 32403

ATTN: HQAFCESA Program Ofc

## US Army Envr Hygiene Agency

ATTN: HSHB-ME 21010

## US Gov't Printing Office 20401

ATTN: Rec Sec/Deposit Sec (2)

## Nat'l Institute of Standards &amp; Tech

ATTN: Library 20899

## Defense Tech Info Center 22304

ATTN: DTIC-FAB (2)

83

7/94